Graphene Encapsulation for Cells: A Bio-Sensing and Device Platform

by

Shehan Salgado

A thesis

presented to the University of Waterloo

in fulfillment of the

thesis requirement for the degree of

Masters of Science

in

Chemistry - Nanotechnology

Waterloo, Ontario, Canada, 2014

Author's declaration

I hereby declare that I am the sole author of this thesis. This is a true copy of the thesis, including any required final revisions, as accepted by my examiners.

I understand that my thesis may be made electronically available to the public.

Abstract

The generation of new nanoscale fabrication techniques is both novel and necessary for the generation of new devices and new materials. Graphene, a heavily studied and versatile material, provides new avenues to generate these techniques. Graphene's 2-dimensional form remains both robust and uncommonly manipulable. In this project we show that graphene can be combined with the yeast cell, *Saccharomyces cerevisiae,* arguably the most studied and utilized organism on the planet, to generate these new techniques and devices. Graphene oxide will be used to encapsulate yeast cells and we report on the development of a method to electrically read the behaviour of these yeast cells. The advantage of an encapsulation process for a cell sensor is the ability to create a system that can electrically show both changes in ion flow into and out of the cell and mechanical changes in the cell surface. Since the graphene sheets are mechanically linked to the surface of the cell, stresses imparted to the sheets by changes in the cell wall or cell size would also be detectable. The development process for the encapsulation will be refined to eradicate excess gold on the yeast cells as well as to minimize the amount of stray, unattached graphene in the samples.

The graphene oxide encapsulation process will also be shown to generate a robust substrate for material synthesis. With regards to cell sensing applications, sources of noise will be examined and refinements to the device setup and testing apparatus explored in order to magnify the relevant electrical signal. The spherical topography of an encapsulated yeast cell will be shown to be an advantageous substrate for material growth. Zinc oxide, as a sample material being investigated for its own applications for photovoltaics, will be grown on these substrates. The spherical nature of the encapsulated cell allows for radial material growth and a larger photo-active area resulting in a device with increased efficiency over a planar complement. The zinc oxide nanorods are grown via an electrochemical growth process which also reduces the graphene oxide sheets to electrochemically reduced graphene. XRD analysis confirms that the material synthesized is infact zinc oxide. The nanorods synthesized are 200nm to 400nm in width and 1μm in length. The increase efficiency of the non-planar device and the effectiveness of the encapsulated cell as a growth substrate indicate encapsulated cells as a research avenue with significant potential.

Acknowledgements

I would like to thank Prof. Vivek Maheshwari, my supervisor whose focus and guidance lead me to new avenues of thought and analysis and who provided support, mentorship and a clear head for understanding and getting through those research road blocks.

I would like to thank my Advisory Committee, Prof. Marc Aucoin and Prof. Shirley Tang for their help and understanding over the course of my Master's progress.

I would like to thank Dr. Nina Heinig for her help and guidance in the use of FESEMs, XRD, AFMs, allowing me to sneak in to WATlabs to test samples past regular hours and allocating our lab group far more than its fair share of time in WATlabs.

I'd like to thank Prof. Juewen Liu allowing me use of his laboratory and help with his equipment.

I'd like to thank my lab mates, Long Pu, Abdulrahman Babatin, Jasper Tam and Mark Miltenburg for their assistance and comradery in the thick and thin of lab work.

Table of Contents

List of Figures

1.0 Chapter 1- Introduction

The development of new techniques, be they for analysis or fabrication purposes, is a critical issue in nanotechnology. Graphene, a heavily studied and versatile material, provides new avenues to generate these techniques. Graphene's 2-dimensional form remains both robust and uncommonly manipulatable. In this project we examine the applications of graphene in combination with baker's yeast, *Saccharomyces cerevisiae* in a number of ways and from a number of directions. This will be done both with the viability of the yeast cell as a concern, for cellular sensing applications, and also from a perspective where the yeast cell is merely providing a robust cellular scale template/substrate. For the first, cellular sensing perspective, we will attempt to generate a prototype system able to convert cellular behaviour, both of ionic exchange into and out of the cell and mechanical changes in the properties of the cell wall, into changes in the conductance of a graphene sheet. For the latter research direction we will explore graphene encapsulated cells as a hybrid substrate for material synthesis, which exhibits the benefit of providing a curved substrate for material growth.

In chapter 2 we give some brief background information on graphene, zinc oxide, *Saccharomyces Cerevisiae,* and the methods and materials that will be used in examining the combination yeast and graphene construct. Chapeter 2 also contains examinations of relavent literature regarding the sensitivity of the system design. Chapter 3 will cover methods and materials used. In chapter 4 we will examine previous work and current modifications to the cell sensor synthesis process. Chapter 5 focuses on the applications of graphene as a single sheet Field-Effect Transistor (FET), converting cellular metabolism and changes in the cell wall into changes in the conductance of a graphene sheet. The encapsulation method used to link the graphene to yeast is refined and the measurement techniques being used to ascertain its behaviour are explored. In chapter 6 we report on graphene encapsulated yeast as a material synthesis substrate. The combination of the curved surface morphology of a yeast cell with the functionalizability and versatility of graphene is explored through a method to synthesize zinc oxide, another material being explored for its potential as an n-type charge carrier photo-generator. Finally Chapter 7 will examine the future potential for the aforementioned techniques and systems.

1.1 Thesis goal- Formation of an electrical sensing prototype

A main objective of this thesis project is the development of an electrophysiological analytical technique for measuring cell behaviour. The proposed method for this development is using a graphene encapsulation process to surround a yeast cell in a conducting layer that will be susceptible to perturbations in its conductance from two sources. The first source is the conductance change due to incident ions from the encapsulated cell modifying the electron density of the graphene. The second source, and the primary reason for mechanically linked encapsulation as a proposed methodology, is perturbations to the conductivity of the graphene from strains on the sheet induced by mechanical changes of the cell itself. Changes in the size of the cell or attempts of the cell to "bud" and develop a daughter cell should both cause mechanical deformations in the cell wall. Graphene's aforementioned flexibility should allow for a mechanically linked graphene sheet conforming tightly to the surface of the cell. It is this ability to act as a transducer for two different behaviours simultaneously that makes the system attractive. In operation, this will be similar in effect to a Field Effect transistor (FET), with an applied voltage sustained across the graphene and the impinging ions replacing a fluctuating gate voltage. To test this fabricated system, a method to electrically read the cell behaviour while keeping the sample incubated in a growth-conducive environment is required. Figure 1 below shows the proposed setup complete with both the cell sensing circuit and the incubation setup to maintain cell viability. In order to sustain the cells, a fluidic cell is used that allows a volume of YPD broth to circuit through a heating area and back into the fluidic housing to maintain a cellular environment of approximately 30°C. In future systems once the prototype is completed, this circulating volume would also allow for the easy introduction of various cell treatments to perturb the cell and measure its response.
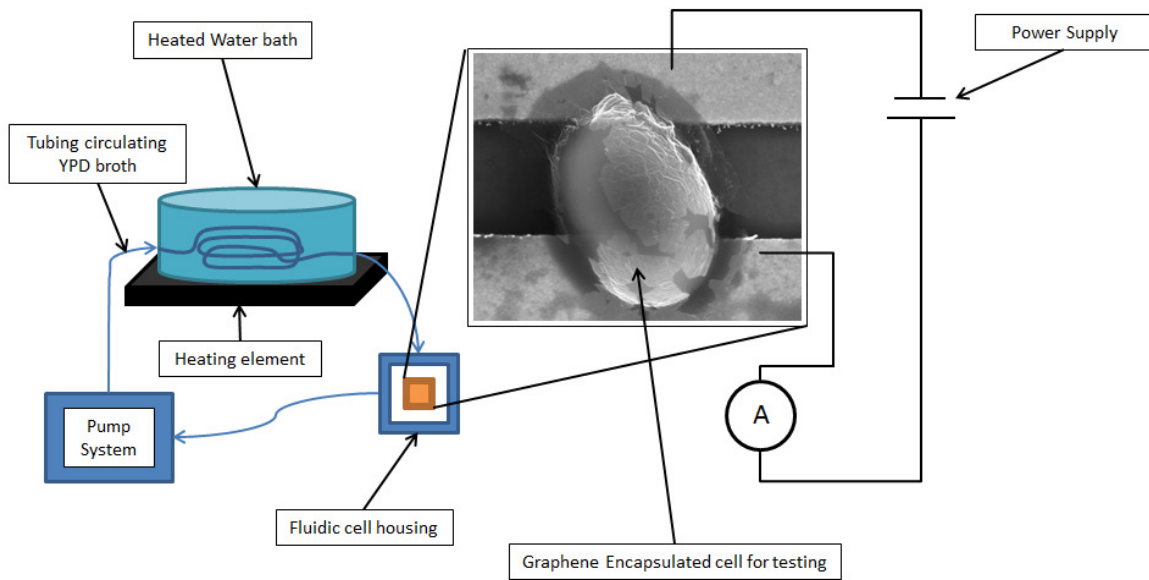
Figure 1: Proposed Cell sensing System, the encapsulated yeast cell (insert) is tested electrically while a closed fluid loop maintains viable cell growth conditions.

1.2 Thesis goal- Examination of GO-encapsulated SaC. cells as a synthesis substrate

An additional goal of this thesis project is to examine the graphene oxide encapsulated SaC. cells as a substrate or template for material synthesis. The cell wall of a yeast cell represents a flexible and curved surface that, in combination with a conducting graphene sheet, could prove an interested and novel hybrid substrate for material synthesis. Most critically, the presence of a curved surface for material growth allows radial growth directions as compared to a planar system.

3

2.0 Chapter 2- Background information

2.1 Yeast Cell- Saccharomyces cerevisiae

The yeast cell, *Saccharomyces cerevisiae* is an extensively studied and characterized eukaryotic cell that forms the basis of a wide range of biological research.[1–3] Indeed the *Saccharomyces cerevisiae* sequencing project was itself completed in 1995, making the yeast cell the first eukaryotic genome decoded.[2] The yeast cell remains a cornerstone of biotechnology for its prevalence, ease of use and robust viability.[4,5] Additional advantages of yeast relating to biotechnology stem from its similarity in subcellular structures to those of multicellular eukaryotes and yeast's well-studied nature.[6] This means there is a wealth of knowledge regarding its biochemistry and molecular biology.[6] The presence of a cell wall and yeast's ability to hibernate through the most adverse of conditions make it an excellent starting point when attempting to design and elucidate new cell sensing methodologies which may affect cell viability during the method development phase.[7–10]

Saccharomyces cerevisiae (henceforth SaC) is a unicellular fungi.[4,5] Yeast cells have been a central part of food production for over 8000 years thanks to their ability to ferment glucose into ethanol and carbon-dioxide.[4,5,8] Yeast species other than SaC are also found on plant leaves and flowers, soil, on skin surfaces and in the intestinal tracts of warm-blooded animals.[5,6,8] *Saccharomyces cerevisiae* multiplies as a single cell that undergoes "budding", a process where a daughter cell is initiated as growth from the mother cell, followed by the steps of nuclear division, cell-wall formation and finally cell separation.[4,5,8] Figure 2 below shows this process, of note are the cell deformation and bud scars the form during the process. While some of the "budding" steps of SaC. are admittedly different to mammalian cells (the formation of a cell wall for one part), SaC. remains a target for research since the base mechanics of replication, recombination, cell division and metabolism are for the most part conserved between yeast and larger eukaryotes, including mammals.[4,5]

The concept of a cell based template, either for cell analysis or for material synthesis purposes, is an idea that has been explored by a number of groups. Cells provide a consistently sized and easily reproducible template on the order of micron scales. If the cells remain viable during the template use process, then this

cell template can be modified or affected with cell signals to adjust the template during synthesis. In particular, yeast's viability is robust due to its ability to hibernate and survive relatively adverse conditions for other mammalian cells due to their cell wall.[9,10] SaC.'s outer most layer is the cell wall, a 70-120nm thick layer composed of polysaccharides (~85%) and proteins (~15%).[3,10,11] This organic composition means the cell is a dielectric and has low thermal conductivity.[3,11] Amino Acids being the basis for proteins, they give the cell wall a net negative surface charge and a negative zeta potential.[3,11] This anionic nature enables the interfacing of graphene oxide with the cell surface via a divalent cation.[3,12]

Figure 2: SaC. cells show bud scars and daughter cell growth[13]

2.2 Graphene

Arguably, graphene as a unique material has been studied for over 60 years.[14,15] In 1947 Wallace investigated the band structure of a single layer of graphite in an attempt to explain its physical properties, including electrical and thermal conductivity, diamagnetic susceptibility, and optical absorption.[14] Since that time, single sheet graphite has gained its own name "graphene", and it and the other carbon allotropes that compose the graphitic forms are well-known and intensively studied for their unique properties and expansive potential.[15–17] Among graphene's critical properties are a high electron mobility at room temperature (250,000 cm^2/Vs), a high specific surface area of 2600 m^2g^{-1}, a thermal heat capacity of 3000$Wm^{-1}K^{-1}$ and an extremely high directional stiffness with a Young's Modulus on the order of 1 TPa. [15–17]

Graphene itself is a 2-dimensional single-layer lattice of sp^2 hybridized carbon atoms that form a bonded planar honeycomb structure.[18,19] Fully filled σ bonds account for graphene's structural strength, key when attempting to utilize it as a robust encapsulating material. [15,18,19] An additional key parameter is the size of the graphene sheets. This large single atomic layer sheet, with a depth of approximately 0.3nm, gives a combination of parameters that leads to a large and flexible monolayer that is able to conform to the topography of the substrate below it. As seen in Figure 3, this ability to conform and deform under stress is a mechanical parameter of graphene's behaviour that will be integral to examining mechanical changes in the cell wall of the yeast cell.[15–17,20] Figure 3 below shows the wrinkling that occurs when graphene is subjected to shear strain, other forms of strain will have similar effects in different axis.
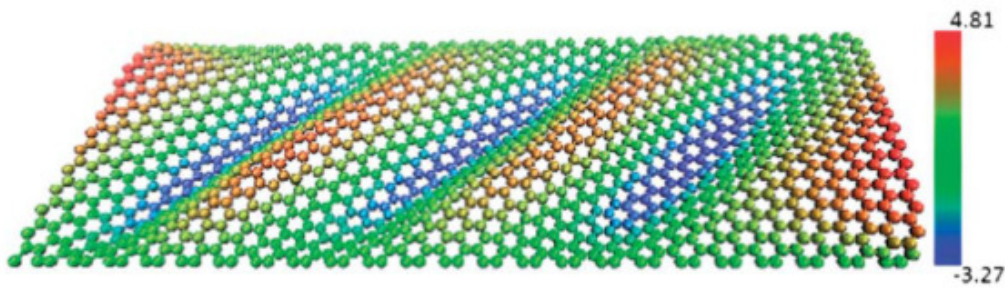
Figure 3: A honeycomb Graphene lattice under 0.216 shear strain exhibits a wrinkle pattern at 300K[21]

The remaining carbon electron density outside of the sp^2 hybridization is held in half-filled π orbitals under the Pauli principle.[22] Graphene's critical ability to conduct as a zero-band gap semiconductor comes from the joining of the σ and π orbitals in two locations in the Brillouin zone.[16,18,22] When this characteristic is combined with its ability to push electrons into the conductance band under a positive bias (when the Fermi level rises above the Dirac point) and allow holes into the valence band under a negative bias (where the Fermi level drops below the Dirac point) the material then demonstrates an ambipolar electric field effect at room temperature.[16,23] Figure 4 below depicts the ambipolar field effect in monolayer graphene, the insets on either side of the graph show how the Fermi level position in graphene (E_F) changes in reaction to the applied gate voltage on the material.[24]

Graphene's electronic character is a significant factor in its prevalence as a material for research. Charge carriers in graphene behave as Dirac Fermions, massless relativistic particles. The ambipolar field effect seen in graphene means that charge carriers can be adjusted between predominantly holes and predominantly electrons, in concentrations of 10^{13} cm^{-2}.[15,25] Graphene's typically excellent long range order also means that this conductivity is reliable; however, these charge carriers can also be significantly affected by defects in their lattice. Lattice defects prevent charge transport and behave as scattering sites for impinging electrons decreasing the material's conductance. [16,22,26,27] This combination of reliability of behaviour with a susceptibility to outside influences gives graphene a unique sensitivity that has potential to allow a single graphene sheet to behave as a field effect transistor (FET). [16,22,26,27]

2.3 Graphene as an FET

Graphene's utility as a Field Effect Transistor or FET is widely studied. The typical conformation of such a device is where a graphene sheet is connected to a source and drain electrode, and a gate "electrode" is either located as a "back gate" on the backside of the substrate or on top of the graphene sheet, known as an "electrochemical gate".[28–30] The latter of these two conformations is more analogous to the proposed design in this project, this is since for the majority of biological systems the sensor system will need to be operated in aqueous solutions and therefore electrochemical gating is a more attractive prospect.[28]

7

When using graphene as the main component of a field effect dependent sensing device, what is being measured is the resistivity, or inversely the conductance, of the graphene sheet. This is electrical detection, when a molecule or charged particle of interest adsorbs onto the FET surface it disrupts the conductance of the underlying graphene sheet, which can be read electrically. Figure 5 below depicts an ion sensitive gating FET. In this system, the solution resistance is ideally small so that the applied gate voltage is across the double layer formed at the graphene-solution interface. The thickness of this layer is dependent on the ionic concentration of the medium. Thus the ionic medium will lead to an amount of ions close to the graphene plane, and thanks to this the electrons and holes in the graphene experience scattering from long range electrostatic interactions. Molecules and ions binding to the graphene change the local dielectric constant, as well as acting as new scattering centers, and thus affect the charge transport in the graphene. Certain molecules could also directly transfer electrons to the graphene, a doping effect. In the system proposed in this project, there is no electrochemical gate and no applied voltage to modify the current characteristics of the graphene, however a change in local dielectric constants and increase in scattering sites seen in this system should still be generated by impinging ions.
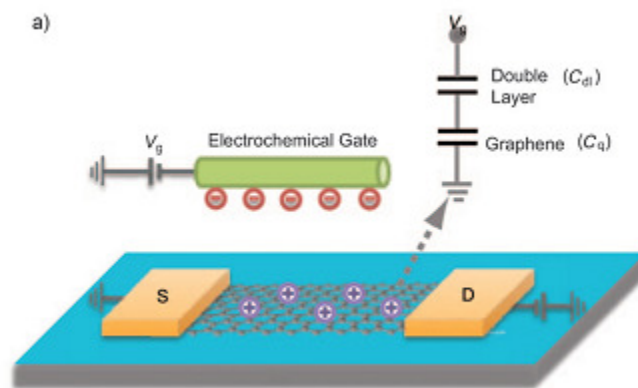
Figure 5: A Graphene sheet connected across source and drain electrodes is able to act as an Ion sensitive Gating FET[35]

2.4 Graphene for Cell Sensing

Nanoscale materials pose new avenues and opportunities for the generation of extracellular cell sensing methods. Unique physiochemical and electrical properties have lead to the development of nanoelectronic biosensors based on a number of the graphitic forms, including graphene. The advantages that nanoscale

biosensors provide are focus in a high attainable sensitivity and high spacial resolution for localized detection.[28,30,31] If the sensing material can be located physically close to what is being sensed presumably a high temporal response could also be elicited from the system.[28,32]

Certainly when taking graphene into consideration, its ease of functionalizability has led to the development of systems using recognition elements to electrically sense behaviour. Biomolecules alter the conductance of the graphene sheet either by inducing an electrostatic gating (field effect) with charged molecular groups or thorough doping effects induced by electron donating or withdrawing groups.[28,32,33] Biomolecules can also possess Carbon rings that can associate with a graphene sheet via strong π-π stacking interactions.[32–34] Dong et al demonstrated these principles in the electrical detection of DNA hybridization by monitoring changes in the conductance of graphene sheets.[33] This was done by immobilizing probe DNA strands on graphene sheets using saturation attachment, it has been determined that the binding between graphene and nucleotides is dominated by the non-electrostatic stacking interaction.[33]

In Dong et al's system, a detection sensitivity of 0.01nM and the capability to detect a single-base mismatch in the DNA was attained.[33] The detection mechanism was the electronic doping of the graphene sheet introduced by target DNA.[33] The transfer characteristics of the graphene sheet were monitored via changes in the gate voltage at minimum conductance of the material. Figure 6a) below shows the schematic for the testing apparatus and an optical microscopy image of the graphene films. The b) and c) fields of Figure 6 show the transfer characteristics for the graphene transistors before adding DNA, after immobilization with probe DNA and after reaction with b) complementary or c) one-base mismatched DNA molecules with concentrations ranging from 0.01nM to 500nM.[33] The results obtained from Dong et al's electrical characterization showed a marked difference in the transfer characteristic when complementary strands, strands able to bind to the adsorbed probe-DNA, are used. The shift in the Gate voltage at minimum current was seen to increase by >10meV and >55meV at 0.01nM and 10nM DNA concentrations, while mismatched DNA only induced a ~20meV shift at much higher concentrations of 500nM.[33] With examinations of the types of shift detected by the system. Dong et al came to the conclusion that the shift seen was due to stacking interactions between the graphene surface and DNA nucleotides and a resulting electron transfer from the DNA molecules.[33]

9
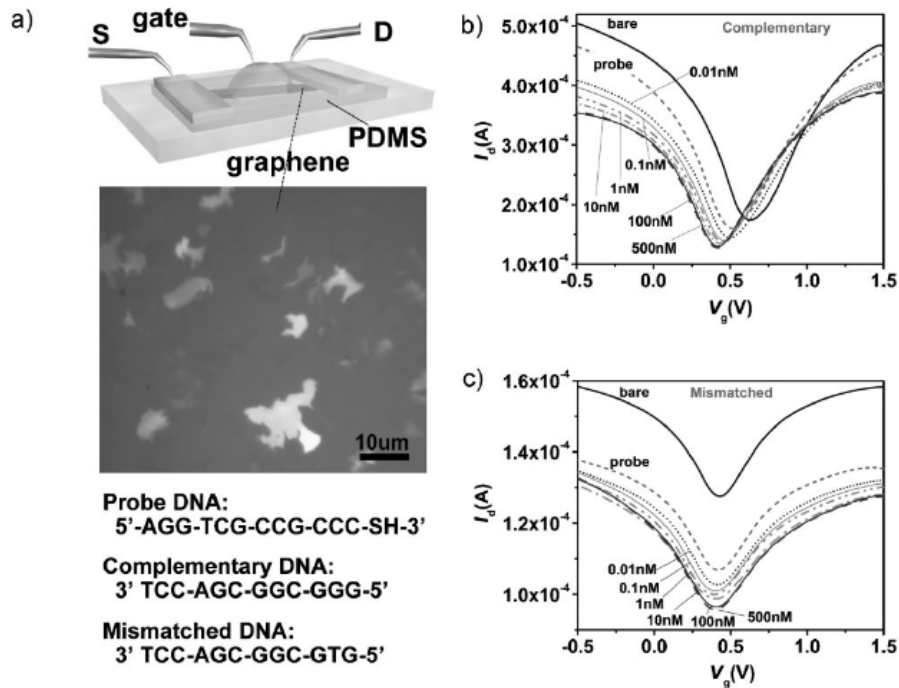
Figure 6: a) schematic of the testing apparatus and optical microscope image of the graphene sheets. b) Electron transference characteristics of the graphene sheet with complementary and c) one base mismatched DNA[33]

Examinations into the sensitivity of graphene for detection while proximal to a cell surface have also been examined. He et al, coupled reduced graphene oxide FET with living neuroendocrine PC12 cells in order to detect the vesicular secretion of catecholamine molecules (dopamine, epinephrine and norepinephrine).[35]

In their system, He et al. generated reduced graphene oxide FET devices and coated the graphene with poly-L-Lysine to make the graphene sheets more attractive as a deposition site for the PC12 cells.[35] After being cultured, a high concentrated K^+ solution was used to elicit detectable responses. K^+ depolarizes the cell membrane and thereby elicits an influx of Ca^{2+} through the voltage gated Ca^{2+} cell membrane channels.[35] This schematic is illustrated in Figure 7.
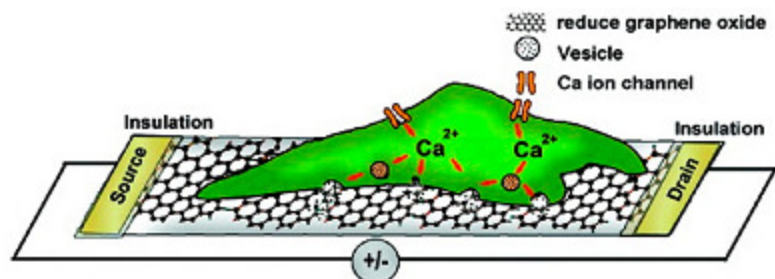
Figure 7: Schematic illustration of the interface between a PC12 cell and a rGO FET.[35]

Figure 8 below shows the collected data for the system. As can be seen, current spikes were detected when K^+ was introduced into the recording chamber. When the cell and functionalized graphene system was exposed to solutions with a high concentration of K^+ ions, the cell membrane would be depolarized and Ca^{2+} would influx through the voltage gated Ca^{2+} channels.[35] Then the vesicular excretions of the cell, specifically dopamine, epinephrine, and norepinephrine would be detected as changes in the conductance of the graphene sheet. A correlation was seen between the release of catecholamines from a single PC12 cell indicating a capability of a graphene FET for applications in electronic biosensing of dynamic cellular activities.[35] The biocompatibility of graphene is of course a concern, and cytotoxic effects have been seen for graphitic materials when they are ingested by a cell, however if the graphene is immobilized as it is in this proposed system (via associations with the cell surface and due to the inherently large size of our graphene sheets), concerns regarding these cytotoxic effects could be largely relieved.[32]
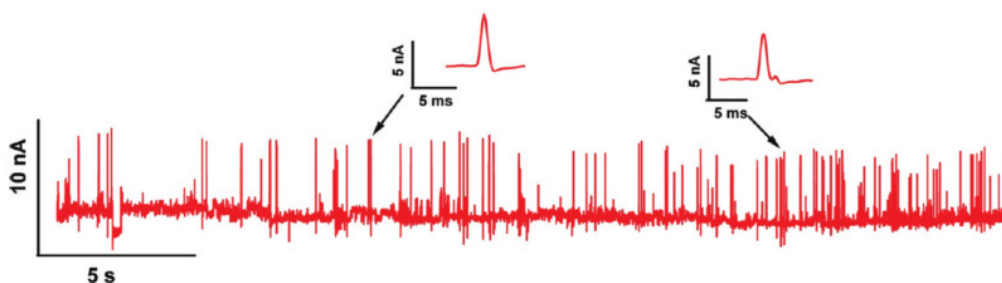
Figure 8: Real time response of rGO-PET FET to the vesicular secretion of catecholamines from PC12 cells stimulated by high K^+ solution.[35]

2.5 Electro-Mechanical Properties of Graphene

The critical difference of the system proposed in this project over the one proposed by He et al. is the existence of mechanical coupling between the graphene sheets and the call wall of the encapsulated cell. This link allows the graphene to not only act as a transducer not only for the detection of ion movement but also for any mechanical changes in the cell wall. This is seen in Figure 9, the left image depicts a cell that is attempting to create a daughter cell underneath the encapsulating graphene layer. This attempted growth will induce strain on the graphene sheet which in turn affects the electrical properties of the graphene sheet. Huang et al. demonstrated a change in the conductance of a graphene nanoribbon stretched and suspended across two gold terminals. A wedge tip structure would be lowered onto the suspended graphene ribbon, inducing a strain. [21]
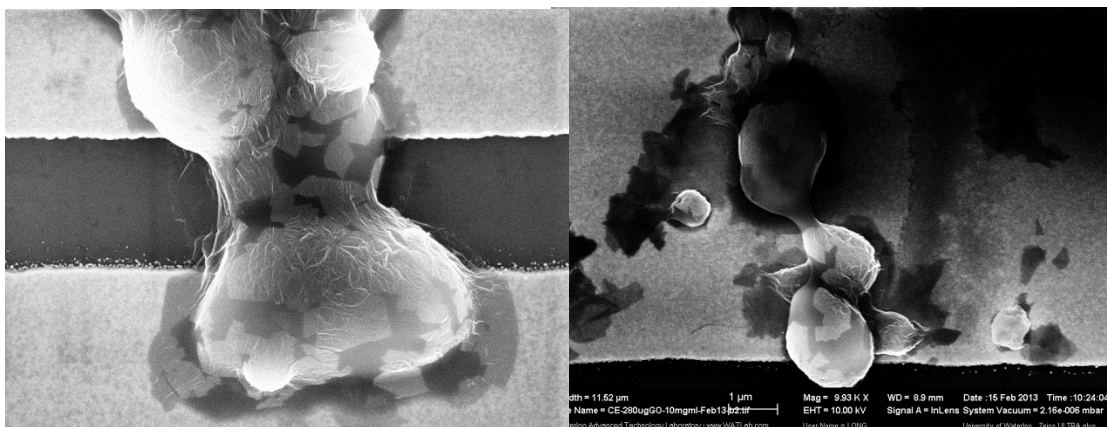
Figure 9: SEM images of Potentially viable cells

2.6 Shell Calculations

In order to ascertain if a graphene sheet encapsulating a cell will be able to detect a change due to ionic flow through the cell membrane, shell calculations were performed to see the required order of magnitude of ionic flow. Yeast extract-Peptone-Dextrose or YPD broth contains 30mM Na Cl and 20mM KCl. In order to calculate the behaviour of the system we calculated the number of atoms that would be required to generate a 10% change in concentration in the volume surrounding the cell at the distance of an encapsulating graphene sheet, approx. 1nm.

Assuming a spherical Cell with a radius (r) of 1μm, the volume of a 1 nm shell around it follows

$$Shell\ volume = 4\pi(r + 1nm)^3 - 4\pi r^3$$

This leads to a shell volume of 0.037×10^{-18} m^3. Knowing the molar concentrations of KCL and NaCl and Avogadro's constant. We can determine that a concentration of 20mM is equitable to approx. 454,123.5 atoms within the 1nm shell.

Therefore the number of atoms that would lead to a 10% change in concentration is 45,412.35 atoms. For the functionality of our device, a graphene sheet encapsulating a cell, and with knowledge of the graphene sheet sensitivity that has been shown to be attainable by Dong et al. in their research, a change in the concentration affecting around 10% of the graphene sheet area should be detectable.[33] This would be expected to be around 4,541.23 atoms.

2.7 Zinc Oxide

Zinc Oxide is a material with a wide variety of applications in electronics, optics and photonics due a convergence of a number of properties.[36–38] ZnO's lack of a centre of symmetry, combined with a large electromechanical coupling results in strong piezoelectric and pyroelectric properties.[39,40] ZnO is a II-VI direct and wide-band gap semiconductor, 3.44 eV at low temperatures and 3.37eV at room temperature.[39–41] Zinc oxide's large exciton energy of 60 meV, significantly larger than GaN's excitons energy of 26meV ensures efficient exciton emission at room temperature and low energy, all of which point to ZnO as a promising photonic material in the blue-UV region.[40,42] This combined with its transparency to visible light and susceptibility to doping makes it an excellent prospect for use in photodetectors and solar cells.[3,36,37] Figure 10 below shows how ZnO's lattice crystallizes in the hexagonal wurtzite-type structure, similar to GaN, with planes of 4-fold tetrahedrally coordinated O^{2-} and Zn^{2+} ions stacked alternatively along the c axis.[39,43] Additionally, ZnO's bactericidal efficacy and anti-bacterial properties increase as its particle size decreases, providing other interesting avenues for research.[36]
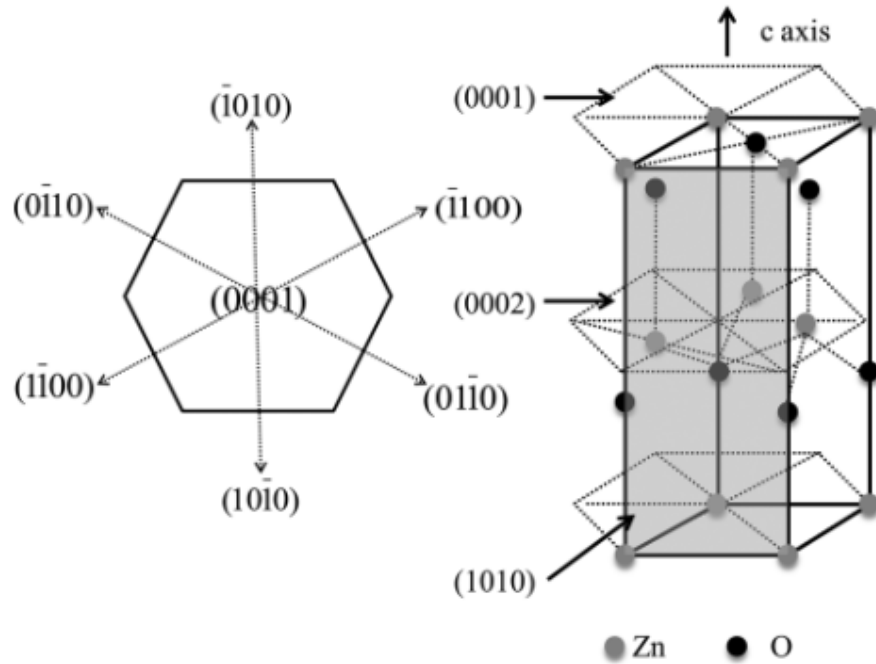
Figure 10: The wurtzite model of ZnO[43]

Zinc Oxide nanostructures are richly varied in morphology, among the most numerous of those used in semiconductor technology.[44] These can include nanowires, nanobelts, nanotubes, nanohelixes, nanorings, and nanorods.[39,40,42,45–48] The typical sensitivity enhancement of high surface-to-volume ratio nanostructures such as nanorods is seen in ZnO as readily as other nanomaterials. There are two main groups of ZnO nanostructure synthesis, spontaneous growth and template based synthesis.[45] The spontaneous growth of zinc nanostructure, particularly nanorods, can occur via a wide variety of methods including gas reactions, solid vapour synthesis, electrochemical growth and hydro thermal synthesis.[39,45] ZnO is usually seen growing along the {0001} c-axis, the vertically oriented crystal axis.[39,43] ZnO films deposited at high temperature are typically oriented with the c-axis perpendicular to the substrate, irrespective of the morphology of the substrate.[36,49] This preferential growth direction is due to side planes of the wurtzite structure being less polar compared to terminal basal planes.[43] The top and bottom surfaces of the ZnO unit crystal are both Zn^{2+} enriched planes and therefore more polar and reactive until a complexing agent compensates for the surface energy, meanwhile the side planes exhibit equal proportions of oxygen and zinc ions and so have no polar component.[43] Figure 11 below shows investigations by Greene et al. into the growth of ZnO. Figure 11a shows the result when growth is initiated by zinc acetate particles while b indicates non-directed growth. In both cases ZnO growth is able

14

to stabilize into growth along the {0001} surface, though the long range order of adjacent rods appears dependent on the initial growth. Without seeds the ZnO nanowires grow disordered, in multiple directions.
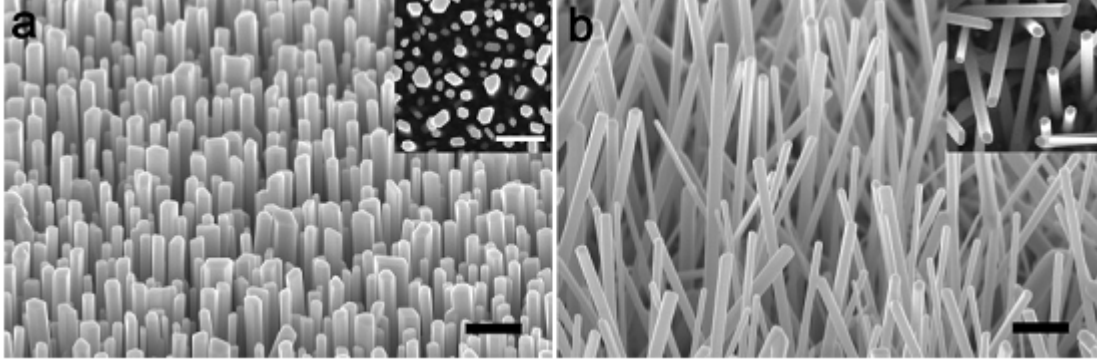
ZnO is an n-type direct bandgap semiconductor with E_g=3.35 eV.[40,42,46] The electron carrier generation that ZnO exhibits is thought to be due to intrinsic defects in the crystal lattice from Zn interstitials. [40,42,46] A popular projected interstitial donor is hydrogen, due to its relevance in most ZnO growth environments.[40] Density-function calculations show that interstitial hydrogens from strong bonds with the O in ZnO and act as a donor.[40] This behaviour of hydrogen is different to its behaviour in other semi-conductors, where it is amphoteric. The stability of ZnO's n-type electrical properties at higher temperatures would also suggest that hydrogen can replace an oxygen in the ZnO lattice and act as a donor in that regard as well.[40,42] Substitutional atomic defects are normally more stable than interstitial defects, so this would explain the stability of ZnO's electronic properties at higher temperatures. These defect levels in ZnO lie 0.05 eV below the conduction band.[46] The room temperature hall mobility of ZnO single crystals in on the order of 200 cm^2 V^{-1} s^{-1}, among the highest mobility seen for oxide semi-conductors.

3.0 Chapter 3 Methods and Materials

There are a number of standard methods and often referred to materials that were used over the course of this project.

3.1 Silanization

Silanization is a standard method by which a surface is covered with a self-assembled layer of alkoxysilane molecules. The reason silanization is used is to make a surface amine terminated, which can facilitate the deposition of various samples for imaging. The majority of the gold interdigitated electrode chips used in this project were silanized to aid with the deposition of reduced graphene or reduced graphene covered cells. The silanization process for a chip, post cleaning with acetone, isopropanol, and Millipore^{TM} water, begins with a 3 minute bath in piranha solution. The piranha solution used was a 3:7 ratio of hydrogen peroxide and sulfuric acid. After the 3 minutes were complete, the chip was rinsed with Millipore^{TM} water and submerged in a solution of 0.98% (3-aminopropyl)-triethoxysilane (henceforth APTES for 10 minutes. Subsequently, after the APTES treatment the chip would be rinsed gently again and heated to 150°C for 30minutes.

3.2 Fluidic Cell

At the center of the testing apparatus of the project is the fluidic cell. This apparatus, designed in house, is composed of 4 screws, a base plate, an o-ring and a top half which houses the well where an incubation solution or deposition solution can rest. In Figure 12 we can see the 3 modifications of the fluidic cell that were used over the course of the project. Beginning with the inlet and outlet form in the top left of Figure 12 and concluding with the no inlet and no outlet form in the bottom. As indicated in the images, as the inlets and outlets were removed from the sides of the fluidic cell they were replaced with tubing entering the well directly from the top. The gold chips used in testing are sandwiched between the top and bottom half of the fluidic device. The sides of the gold chip stick out laterally enabling probe tips to be placed on the gold pads at the side. Appendix A shows a gold chip in depth. An o-ring on top of the chip ensures a tight and gentle seal for the well.
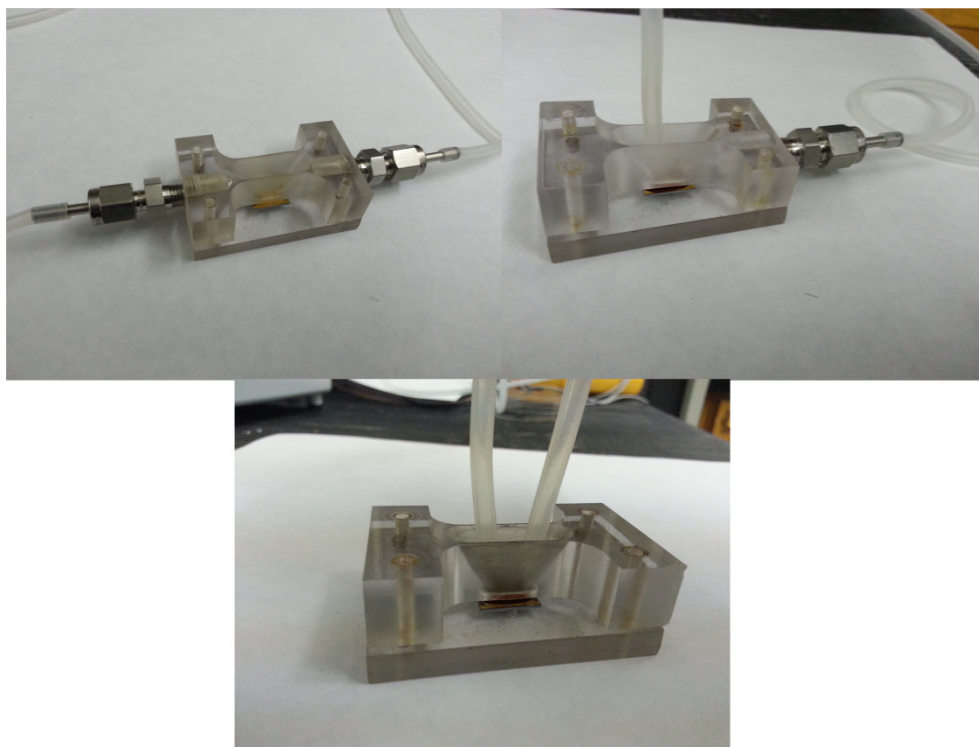
Figure 12: 3 Fluidic cell configurations

3.3 Graphene Oxide Preparation

The graphene oxide used was synthesized utilizing a modified Hummer's Method followed by osmotic dialysis and filtration. Initially, the source graphite flakes (~325 mesh size, Alfa Aesar) were oxidized. 3 grams of graphite flakes were dissolved in 50ml of H_2SO_4 accompanied by 2g of potassium persulfate ($K_2S_2O_8$) and 2g of phosphorous pentoxide (P_2O_5). This mixture was then heated at 90^oC until the components had dissolved and then stirred and heated for an additional 4 hours at 80^oC. After 4 hours 500ml of Milli-Q Millipore^{TM} water was added dropwise to dilute the solution and stirred overnight. This step was executed with caution due to its significant exothermic nature. Subsequently the solution was filtered and washed with Millipore^{TM} water and dried to obtain a pre-oxidized graphene oxide form.[50]

The pre-oxidized graphene form was then suspended in a solution of 125ml H_2SO_4 and 15g of Potassium Permanganate ($KMnO_4$).[50] An ice bath was used during this process to maintain a sub 20^oC temperatures and the solution was stirred for 2 additional hours. Then 130ml of Millipore^{TM} water was added and the temperature of the solution was allowed to raise to 95 degree, upon which an additional 400ml of Millipore^{TM} water was added.[50] After 15 minutes, 15ml of hydrogen peroxide (H_2O_2) was added in order

17

to convert manganese in the solution to manganese sulphate. The addition of hydrogen peroxide and formation of manganese sulphate results in a bright yellow colour. To ensure the reaction is as complete as possible, additional hydrogen peroxide is added in 1ml increments until no additional colour change is registered. The solution was then left stirring overnight. The next day the mixture was washed with 1:10 HCl and filtered to remove any metal ions. The mixture was then washed and filtered with additional millipore[TM] water until a mixture pH of approximately 5 was reached. The mixture is then dried and resuspended as a dispersion of composition 2% w/w. This dispersion was then subjected to osmotic dialysis until the rinse water maintained a pH of approximately 7.[50] The graphene and graphene oxide used and prepared as part of this project are on the range of 0.5µm to 1µm diameter sheets

3.4 Dielectrophoresis

Dielectrophoresis (henceforth DEP) is a manipulation method first introduced by Pohl et al. to describe the translational movement of particles in non-uniform electric fields.[51,52] Currently DEP is a technique that is used in microelectromechanical systems as a way to trap, manipulate and separate bioparticles.[51–53] In contrast to electrophoresis, which is the movement of charged particles in a direct current or low-frequency alternative current field, dielectrophoresis relies on inducing a charge on a sample which is non-uniformly distributed.[51–54] A dipole moment m is induced in a particle, represented by equal and opposite charges (+q and-q) at the particles boundary. [52] The magnitude of the induced charge q is around 0.1% of the net charge usually carried and critically, the charge is non-uniformly distributed over the surface of the particle, creating a macroscopic dipole.[52] When an applied electric field to the particle is non-uniform the resulting force on the particle will be different depending on its size and shape, therefore, it will be induced to move to where the electric field is weaker or stronger, positive or negative DEP respectively.[52] Figure 13 below shows a sample schematic by Dimaki et al. for a carbon nanotube with an induced dipole moving towards the area of high electric field, similar to the method of DEP used in the Maheshwari lab for DEP of graphene and graphene oxide. In Figure 13 the carbon nanotube immediately aligns to the electric field lines and, under positive DEP, moves towards the substrate surface.[54]
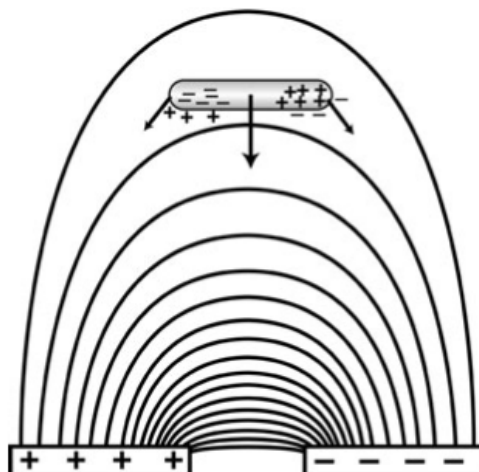
Figure 13: The electric field generated and forces induced on a Carbon nanotube during diaelectrophoresis (DEP)[54]

3.5 Gold Chip

To enable testing of the various samples over the course of the project, a gold-silicon chip was developed. These chips feature interdigitated electrodes which provide 2μm wide gaps between 5μm wide gold fingers as a "gap" samples can be tested across. To ensure that a chip with no sample on it will not conduct, the surface of the chip (immediately below the gold electrodes as well) is a SiO_2 Layer of a depth of 200nm. These chips were used extensively over the course of the project. A schematic of their design can be seen in Appendix A.

3.6 Yeast Cell growth

The yeast cells used in this project were grown via standard incubation techniques. Yeast-peptone-dextrose (YPD) broth was used to grow and harvest the cells. To prepare the cells, 2 grams of powdered YPD would be dissolved into 40ml of Millipore water and autoclaved to sterilize the solution. Subsequently, SaC. of the strain BY4741 were grown at a temperature of 30-31°C in a water bath shaker for 8 hours until the cells reached a point of logarithmic growth and peak metabolism. To remove the cells from the YPD broth they were centrifuged for 30 seconds at 3000RPM and washed with Milli-Q Millipore™ water. This step would be repeated twice to ensure that the Yeast cells were completely free

of the YPD broth. In each wash step, the cells would be resuspended in 0.5ml of Millipore[TM] water and 2 vials would be combined to concentrate the sample. These steps constitute the formation of the "stock" yeast cell solution that would be the basis of the synthesis methods in this project.

3.7 Zinc Oxide growth

An electrochemical process was used for the generation of ZnO nanorods. The synthesis was conducted across the gaps in the gold electrode array chips mentioned previously. The substrate for the process would be material in contact with the working electrode of the gold array or the working electrode itself. Once an appropriate chip and specific gap were selected, the chip was housed in a thermally conducting fluidic cell similar in design to those seen in Figure 12 but composed instead out of a thermally conducting polymer. After confirming that an electrical connection was present on the selected array gap, this construct would then be heated to a temperature of $75^{\circ}C$ using a hot plate, and filled with a solution of 0.1M KCl and 1.125mM $ZnCl_2$. The working electrode was maintained at a bias of -0.955V with respect to an Ag/AgCl reference electrode. The counter electrode, to complete the three electrode set-up, was an adjacent gold pad. Synthesis at the applied voltages was applied for a duration of 4-10 minutes depending on the experiment in question. A schematic of the setup in question is provided in Figure 26 as well as the overall proposed process.[3]

3.8 Instrumentation

A number of analytical techniques were used to characterize the samples generated. The FESEM images collected were obtains using a Zeiss Ultra Plus Field Emission Scanning Electron Microscope (Henceforth FESEM) with a Gemini 1 column.

XRD data was collected using a Panalytical MRD Pro with a 0.27 Parallel plate Columnator and X-ray Mirror in Linear mode.

4.0 Chapter 4- Cell sensor synthesis methods

4.1 Previous development

Figure 14 demonstrates the starting point of the project. As can be seen, the initial solution phase synthesis process results in stray graphene. In order to construct a functional device a critical concern was the eradication of this stray graphene.
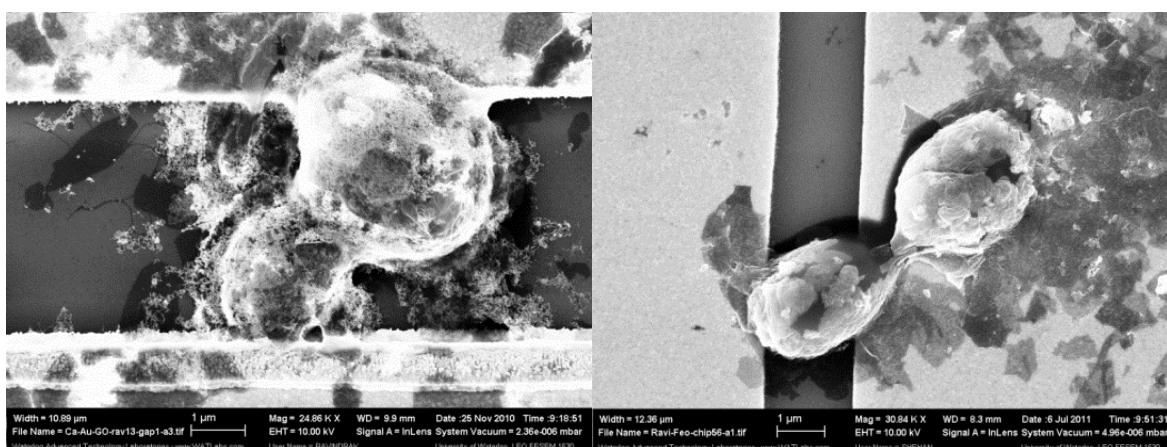
Figure 14: Previous work on the cell encapsulation process demonstrates the two initial issues, a) Excessive Gold deposition and b) Excessive Graphene deposition

The solution phase process developed by Kempaiah et al. while resulting in robustly attached graphene sheets, also results in a large amount of free floating, Au nanoparticle covered graphene that can deposit concurrently onto the gold electrode array along-side the graphene covered SaC.[55] In order to attain an accurate signal from the graphene covered SaC, eradicating this superfluous graphene was critical as, if located within the same interdigitated electrode array, it would provide alternative pathways for current to flow relatively unimpeded compared to the graphene covered SaC and thus obscure the graphene-cell signal.

4.1.1 Final Method

The synthesis process began similarly to the process outlined by Kempaiah et al. with approximately 360µl of a (1mg/ml) CaCl$_2$ being added to 4ml of gold colloid solution (10nm, BBI International) and stirred for a minimum of 8 hours. Upon the addition of CaCl$_2$, dissociated Ca^{2+} ions associate with the COO$^-$ ions present on multiple Au NPs and form Calcium Citrate [Ca(RCOO)$_2$]. The divalent nature of Ca^{2+} then allows the association of multiple Au NPs and leads to the formation of Au NP chains. After a minimum of 8 hours the Au NP solution transitions from a purple colour to dark blue indicating the formation of chains. Figure 15 below shows the mechanism for the formation of gold nanoparticle chains and the resultant colour change.[56]
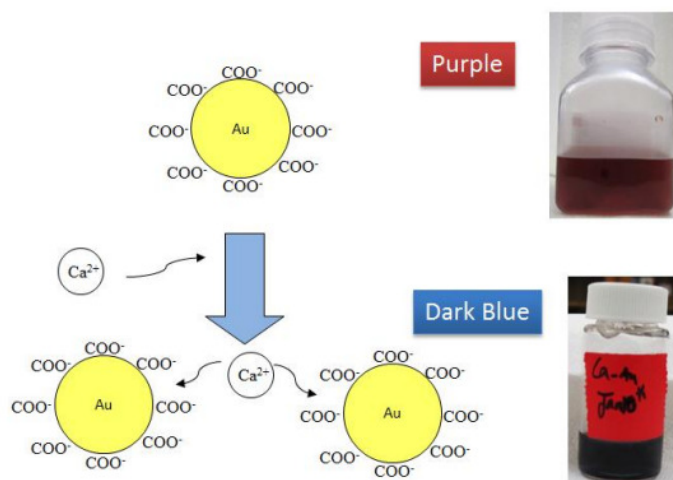
Figure 15: Gold NP chain synthesis process. Citrate ions on separate Au NPs each associate with divalent Calcium ions to form linked chains.[56]

In contrast to the original method by Kempaiah et al., where exfoliated graphene oxide would be added at this step, instead 800ul of purified SaC. suspended in autoclaved Millipore^{TM} water was added to the solution.[12] The reasons for this divergence were multi fold. The Au NP chains are an excellent linker to both graphene oxide and SaC. Unfortunately, a linkage issue that arises is that this linkage affinity can result in Au NP chains that attach between graphene oxide sheets instead of to both a cell and a graphene oxide sheet. The same versatility of attachment that makes the Au NPs critical to synthesis prevents them from constraining their attachment. Thus when the cells are finally added to a graphene oxide and Au Np solution, two types of counter-productive (from a device perspective) linkage are observed. Figure 14, shows a graphene oxide coated cell presenting superfluous and unnecessary Au NP on the outside of the structure, other examinations have shown a cell with multiple layers of graphene oxide attached. Both of

these behaviours are counterproductive to the formation of an elegant and minimalistic device. Therefore a process change was made allowing the yeast cells to attach to the Au NP chains initially. These Au NP-SaC. could then be centrifuged out of the Au NP chain solution and resuspended in autoclaved Millipore^{TM} water to yield a solution containing Au Chain "functionalized" SaC. The reason for not trying a centrifugation and resuspension of the graphene- Au NP solution was to avoid the multi-sheet graphene oxide and Au NP agglomeration that could form when attempting to centrifuge down Au NP-graphene oxide. Comparatively it was presumed that any yeast cell to yeast cell attachment that could occur via Au NP should be comparatively easy to sever during standard resuspension procedures. While not actively searched for, the issue of irreversible cell-to-cell attachment was never observed and large cell agglomerates were not observed in high enough numbers to impact the deposition and testing of single graphene covered cells.

As can be inferred, subsequent to the addition of the cell suspension to the Au NP chain solution and a 30min incubation time, the solution was centrifuged at 3000 RPM for 30 seconds. Then the supernatant (still the blue NP chain suspension) was removed and disposed of while the white cell precipitate was retained and resuspended in autoclaved Millipore^{TM} water. As this results in a concentrated cell solution, this was then diluted with an equal proportion of autoclaved Millipore^{TM} water, for a typical final volume of 6ml, and to this 800µl of 1mg/ml $CaCl_2$ was added. This solution was allowed to incubate for 30 minutes before the addition of 160ul of centrifuged and non-reduced graphene oxide. Prior to being added, the graphene oxide synthesized via the modified hummer's method was sonicated for 5 minutes and centrifuged at 3000 RPM for 3 minutes to remove any large graphene agglomerates present in the precipitate after centrifugation. The decision to use non-reduced graphene oxide over the partially chemically reduced graphene oxide noted by Kempaiah et al. was due to the requirement to attach the graphene to the Au NP chain covered SaC.[55] Cells incubated in the Au NP solution do not attach to the Au NP chains as readily as partially reduced graphene does, resulting in dramatically lower amounts of Au NP chains present on the cell walls of the SaC. as compared to that seen by Kempaiah et al. in their method. Figure 16 shows a standard encapsulated cell bridging a gold chip gap. The amount of Au NPs present on the sample is severely reduced, only the amount required for attachment is present. As mentioned previously, in order to eliminate stray graphene sheets which make accurate readings difficult, this modification to addition order in the procedure was necessary. However the partially reduced graphene oxide used by Kempaiah et al, was unable to attach in sufficient numbers so as to preserve the final encapsulation configuration when used in the new procedure.[55] Switching back to non-chemically reduced graphene oxide alleviated this problem and allowed adequate levels of graphene oxide coverage.

Non-reduced graphene oxide was able to bind much easier to the Au NP-SaC hybrid. However, this would result in the requirement of a further reduction step further down the line in device fabrication. Figure 17 below depicts the entirety of this new GO attachment process.
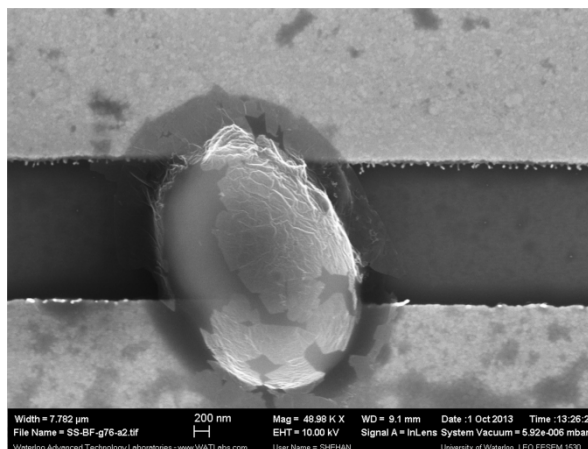
Figure 16: Resulting Cell coverage typical of the new attachment process

After the addition of the graphene oxide, the incubation time was extended by 30 minutes, followed by two additional centrifugation steps, each at 3000RPM for 30 seconds and each followed by the removal of the supernatant and resuspension of the cells in autoclaved Millipore^{TM} water. These were performed to further reduce the amount of stray graphene present in the final solution, before the sample was depositied on a gold patterned silicon chip (Appendix A). Deposition was performed by simple solution phase deposition for 15 minutes. Subsequently the graphene oxide encapsulated SaC solution was stored in a freezer at -20°C. This stored solution could then be used at a later date to deposit onto additional gold chips for testing.
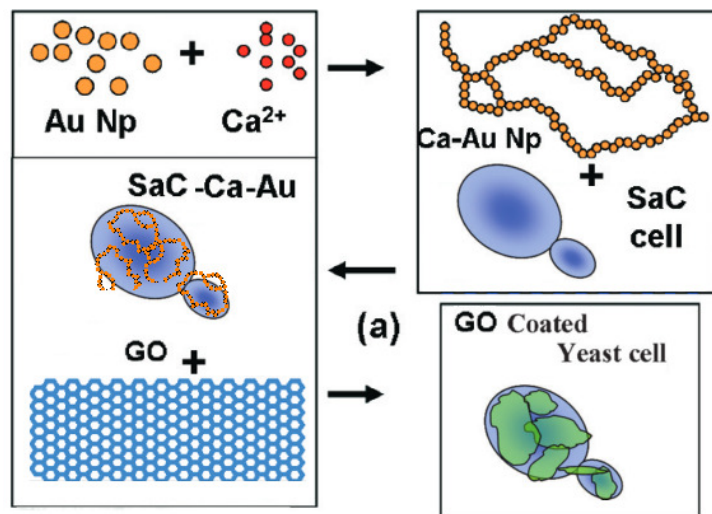
Figure 17: The new cell encapsulation methodology begins with the association of Au NP chains with the cell surface via Calcium ions. Then, aqueous graphene oxide associated with these Gold covered yeast cells[12,56]

5.0 Chapter 5- Cell Sensor characterization and development

Figure 23: , depicts the testing system. In the final device testing setup a variable speed peristaltic pump is used to circulate broth around an open loop and through a fluidic cell. Sterilized silicon tubing is used for circulation. A water bath is heated and maintained at 46°C to maintain a broth temperature of 30°C in the fluidic cell. The total circulation volume is dependent on the length of tubing, and to minimize the mass requirement to reach critical concentration thresholds during treatment application this length should be kept to a minimum. In our final device setup this flow volume was 4ml.

5.1 Cell survivability

The viability of cells that have undergone the encapsulation process is paramount, as in order for this system to be translated onto other more fragile cell systems at a later date, a yeast cell, a cell that is comparatively robust, must be able to survive the process. Figure 9: SEM images of Potentially viable cells, below, depicts cells we believe may be attempting to reproduce either during or after the graphene encapsulation component. The left figure shows a yeast bud growing in the bottom center of the image directly under a graphene sheet, while the right most image shows two cells on the cusp of separating perhaps.

5.2 DC Testing

Initial testing on the device was performed with an applied DC current. When testing the graphene covered cell device, care needed to be taken to ensure the signal read was in fact due to the current passing through the graphene layer on the surface of the modified yeast cells. Since testing is performed in a broth solution (to facilitate cell health and growth) if the applied voltage is erroneously high during testing faradic reactions can occur on the gold electrode exposed to the broth solution. In order to minimize this effect in testing, a gold chip with no material bridging the gap was tested at a number of voltages to read the resulting current. Significant spikes in the measured current occurred when the applied voltage on the sample reached over 0.3V. It was assumed that this was due to the formation of

faradic reactions at higher voltages and so moving forward, testing was constrained to voltages of 0.3V or lower.

5.3 Periodic Noise reduction

The physical design of the testing apparatus was itself an iterative process. Figure 12 shows the 3 different schematics that were designed over the course of the project. The initial design shown in the top left depicts the starting point of the project. The fluidic well is designed to isolate the interdigitated electrode section of the gold chips from the probe pads so that the gaps of the interdigitated electrodes could be exposed to various treatments. In the initial design parameters we wished to avoid any "dead volume" during pumping, a volume of the flow that does not circulate with the rest of the fluid. To deal with this, the initial design had the inlet and outlet of the well of the fluidic cell enter through the sides of the top plate, elevated approximately 3mm above where the surface of the gold chip would be during testing. Figure 18 shows a preliminary examination using a DC applied voltage to measure cell behaviour over an extended time period. The sample in question is a graphene oxide encapsulated cell typical of the samples which were examined over the course of the project. However in Figure 18 we see a periodic downward spike in the measured current of the system, occurring on a 40 second period, and masking and obscuring the presumed signal of the sample itself. These signal spikes were not initially seen during an experiment but could either spontaneously occur during a test, after which they would not cease, or they could be induced if the sample was disturbed physically. After being induced or spontaneously generating the periodic spikes would not cease unless the circular flow of the system was either severely reduced or cut off entirely by shutting off the pump.

GO- Encapsulated Cell Regrowth Attempt
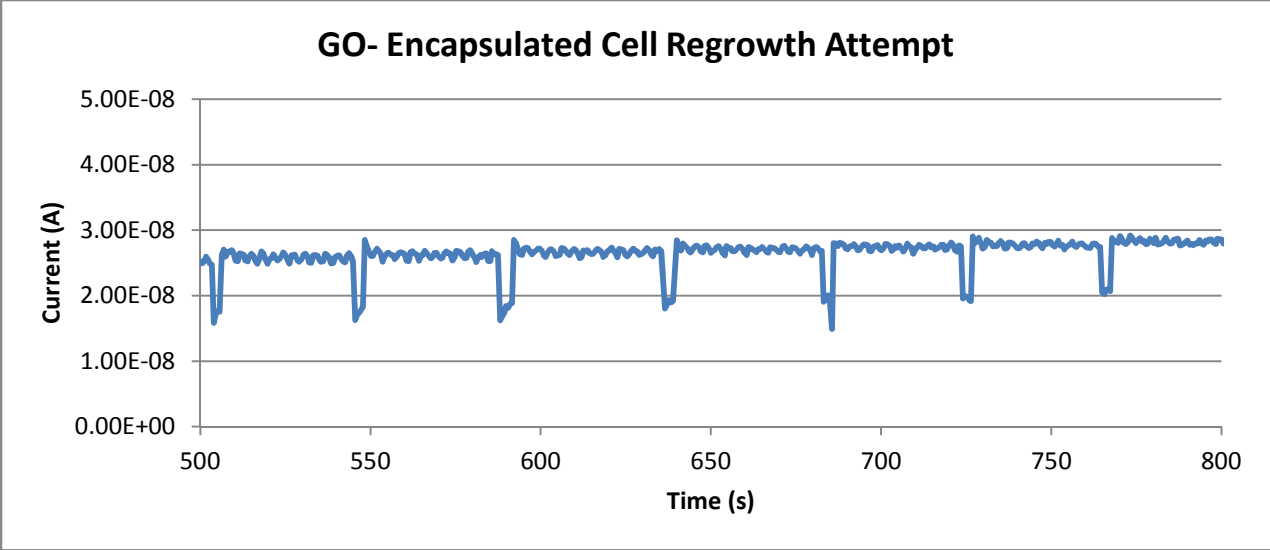
Figure 18: DC Regrowth current data, a single encapsulated cell's response over time to a 0.25V applied voltage

To remedy this, modifications to the system were made to use regulate the pump into a more continuous flow configuration. Modifications were also made to the design of the fluidic cell. Initially the inlet of the system was removed and instead the rubber inlet tube was suspended above the well, allowing the fluid to flow into the well from the top. Eventually, in order to completely isolate the sample from as many pressure waves of sporadic flow as they could be both the inlet and outlet were removed from the fluidic cell itself and instead the inlet and outlet tubing lines were both suspended above the well. This is the current configurations of the system used to date.

5.4 Signal Isolation- Lock In amplifier

During testing, it was noticed, as show in Figure 18, that the magnitude of the signal obtained during regrowth testing was significantly high, by an order of magnitude if not more, than what is observed in the pre-testing characterization of the sample. Prior to running the extended Time-IVs on the prepared samples the electrical connection across the sample is double checked to ensure that the "gap" in question conducts properly and on an expected magnitude considering the material bridging the gap. Figure 19 below depicts a standard air IV curve typical for a graphene encapsulated cell sample. The graphene on

the cell has been reduced. As can be seen in Figure 19 the typical values expected for a single graphene encapsulated cell below the critical value of 0.3V is in the 2.5-3 nA range. This value is an order of magnitude smaller than the approximate 28nA seen in Figure 18. It is likely that this disparity is due to effects of the YPD broth composition on the graphene. In order to separate out the critical important data from the sample we required the use of a lock-in amplifier.
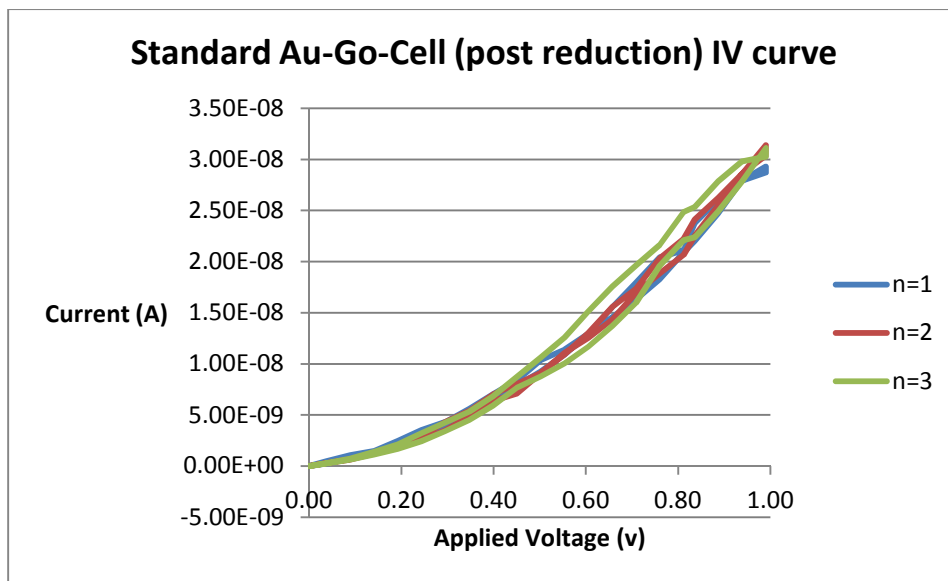
Figure 19: Standard IV curve in Air for Encapsulated cells across an array gap.

In a lock in amplifier, phase sensitive detection is used to single out the component of a signal at specific phases and frequencies in response to an applied signal at a specific frequency. Intuitively the response signal of the system should have the same frequency as the applied signal, though whether the response is resistive or capacitive the phase of the response could change. The utilization of a lock in amplifier is the next step for this project

5.5 Explored "post assembly" graphene oxide reduction methods.

As mentioned previously, a significant design change was the switch from using pre-reduced graphene to unreduced graphene oxide in the encapsulation process. The advantage of this process was a higher

quality of attachment chemistry and less free floating graphene in the samples. However, in order for the proposed device to function at peak operation it is critical that the graphene sheets attached to the cell surface are in fact graphene and not graphene oxide, or at least as close to that ideal as is possible. In our system, we wish to measure the operations of a living cell by linking the disruption and changes in graphene's conductivity to the movement of ions into and out-of the encapsulated cell. Having the yeast cells encapsulated in reduced graphene maximizes its conductive ability and ensures that the signal response of the system can be maximized. Graphene oxide's epoxy, hydroxyl and carboxyl groups disrupt the sheet wide field of electron density that is critical to graphene's operation. If the encapsulating graphene oxide is reduced, then the conductance response for the sample should be that much more pronounced a diversion from the norm.

A hurdle encountered at this point was the requirement to successfully reduce the graphene oxide on the sample without damaging the underlining cell. In order to translate this measurement methodology to applications on other cell types in the future the proposed methods would need to be comparatively gentle. Typical methods utilized in the lab, such as thermal reduction, or hydrazine vapor reduction, would be much too violent methods to attempt to use on the encapsulated cell constructs while maintaining cell viability. Since damaging the underlying yeast cell was not an option, a simple method for graphene reduction was explored, photo reduction.

Graphene oxide's UV-Vis spectrum has two distinct features that can be used to identify it and examine its degree of functionalization.[57–59] Congruent to both Graphene and graphene oxide is the $\pi\rightarrow\pi*$ transitions of the aromatic C-C bonds, the maxima of the spectrum is at 231nm.[58] Additionally, the C=O bonds in graphene oxide cause the presence of a "shoulder" at 300nm that extends to 320nm, this due to the n$\rightarrow\pi*$ transitions.[58–60] This composes the characteristic UV-Vis structure of graphene oxide. Figure 22 below depicts our UV-Vis data for the source graphene oxide we generate via our modified Hummers method, and the spectra for chemically reduced graphene, reduced from our source in the solution phase with hydrazine and ammonium hydroxide.
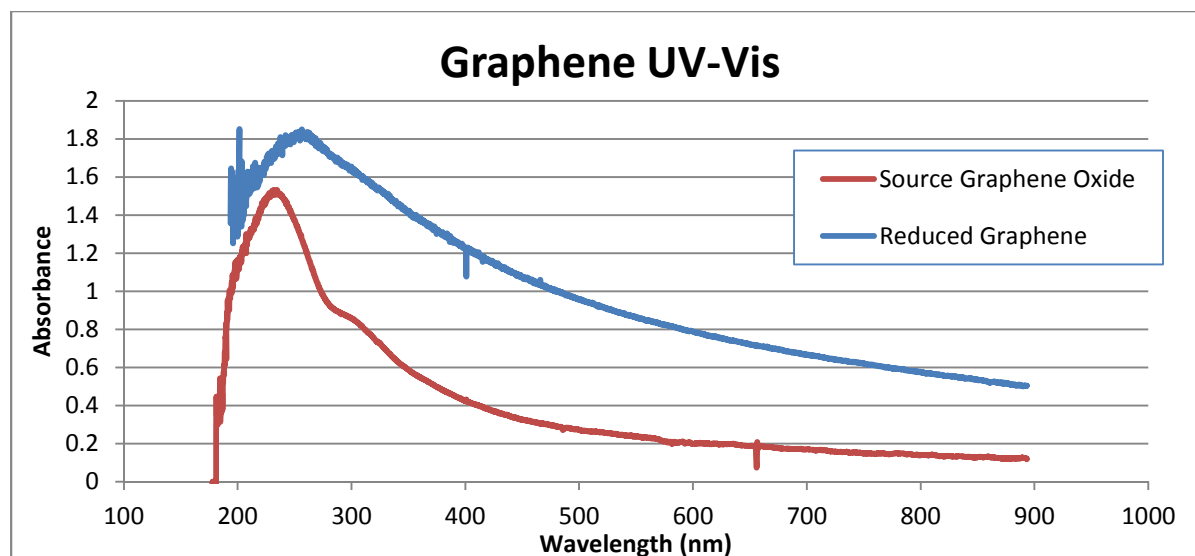
It is known that the absorption of graphene oxide in its range can lead to a high temperature and reactive environment conducive to deoxygenating GO.[57] Typically when this effect is used to attempt to reduce graphene oxide, the process is facilitated by a photo catalyst, such as TiO_2, though the process can also be facilitated in a self-photo catalytic reduction strategy, usually in the company of an electron donor.[59] We attempted to actuate the self-photocatalyzation of graphene oxide by exposing it briefly to light at the wavelength of 620-650nm generated with the Cy5 excitation filter of LEICA DMI3000 B and a fluorescent light source. The beam of the microscope was focused onto the particular gap in question. It should be noted that this process is typically not used since the excitation of GO can lead to the breaking of carbon-carbon bonds which would lead to defects in the graphene.[57]

Figure 21 shows the degree of reduction attained when a graphene sample was subjected to multiple exposure profiles and finally heat treatment. The graphene sample was prepared by placing a cleaned and silanized gold chip in a fluidic cell and filling the well with400 fold dilution of 2% graphene oxide solution, A specific gap, chosen for its cleanliness was then exposed to a 2MHz and 500mV AC applied voltage for 10 minutes. The sample was examined under a LEICA DMI3000 B microscope to confirm the success of graphene oxide deposition to that specific gap. In Figure 21, we see the original, pre-reduction current is 1.2nA at 2 V, comparatively the result after exposure to the 320nm beam is significantly higher.

31

At 21nA, the two minute exposure time does indicate some level of reduction, however this value doesn't seem to increase when the exposure time is quadrupled to 8 minutes. While initial results looked promising, the subsequent heat treatment of the sample showed otherwise. Thermal elevation is demonstrated to reduce graphene oxide to graphene successfully and so this method was used as a benchmark to gain a rudimentary measure of the degree of reduction that had been obtained.[61,62] This was performed by elevating the temperature of the gold chip to 200°C for 30 minutes. Unfortunately, as can be seen in Figure 21 on the secondary axis, there is still a significant distance to be covered in this technique before it could be used as a reduction method. Currents obtained with the heat treatment of the chip are on the order of 20000nA, far from the 20nA obtained with the UV reduction.

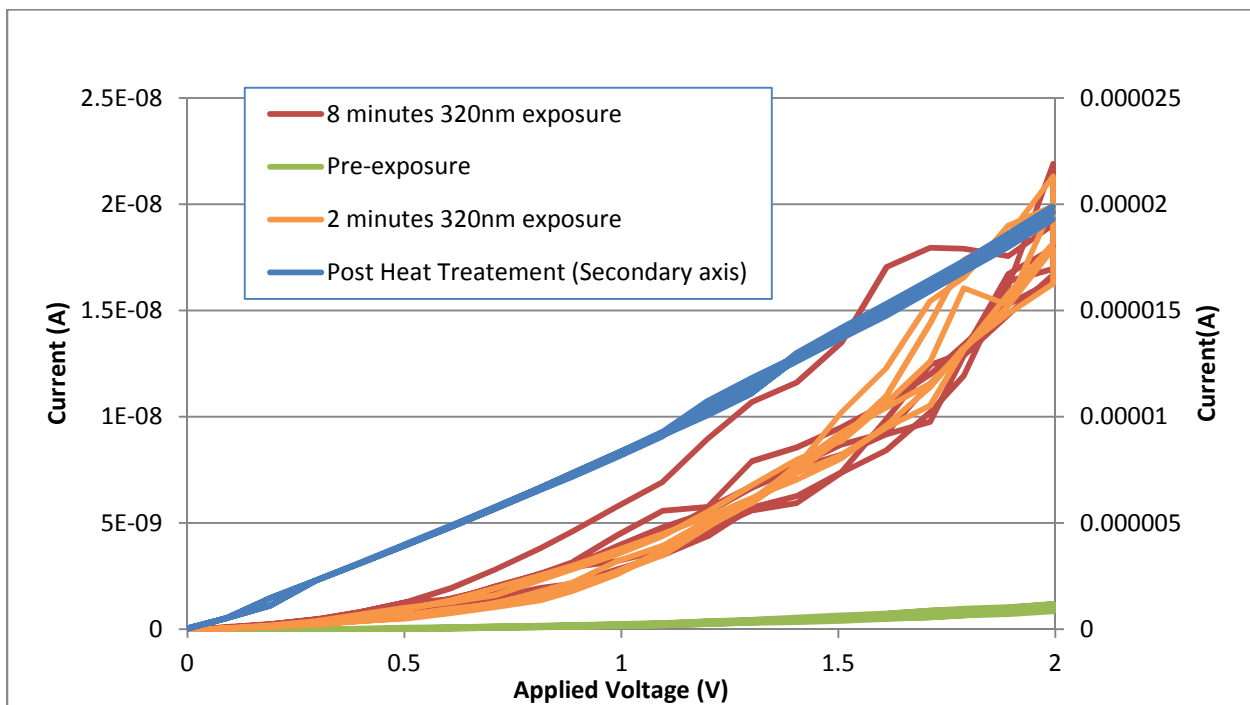Figure 21: Impact of UV Reduction of Graphene as compared to thermal reduction methods.

5.6 New device design schematic

With the difficulty we were experiencing in attempting to reduce the graphene oxide encapsulating a cell sample after encapsulation an alternative methods was proposed in the interim with which we could attempt to move forward on the characterisation portion of the project while other reduction methods

32

were researched. While the aesthetics of a self-contained, single cell testing system are pleasing, that is to say, having a single cell encapsulated in graphene and testing for behavioural changes, the ultimate goal of the project is to attempt to measure the behaviour of a cell via its impact on the conductance of a graphene sheet in close proximity to its surface. To that end, a multilayer encapsulated cell and "free" cell system was proposed as an interim method. The end result of this is shown in Figure 22.
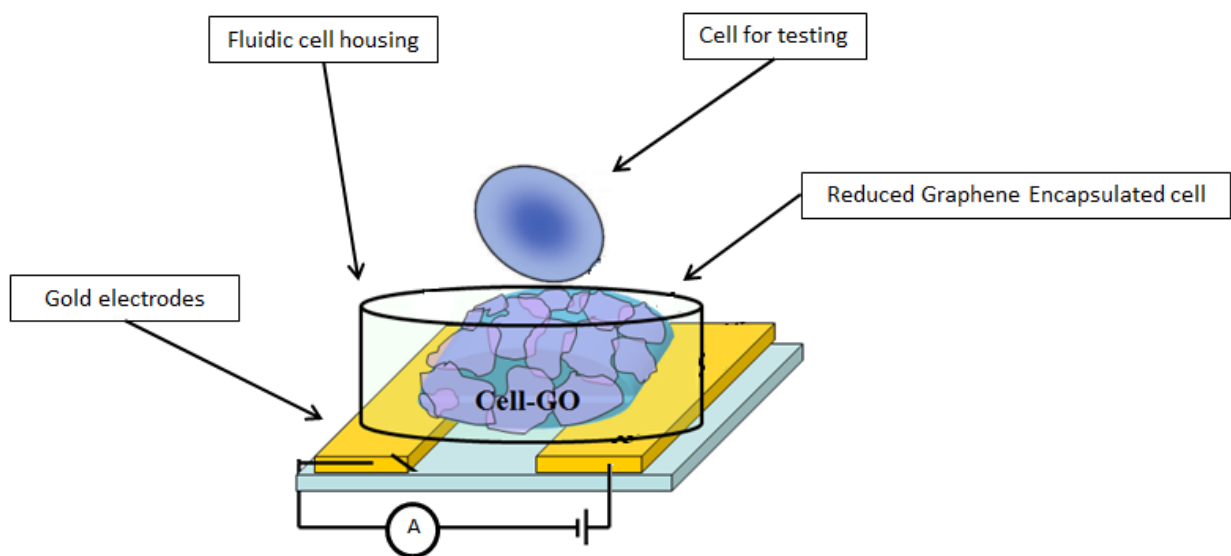
Figure 22: Cell-on-cell device schematic

In this method, graphene coated cells are exposed to the electron beam present in the FESEM, this allows us to both locate good gaps for testing and additionally reduce the graphene on the cell sample from graphene oxide to graphene. A "good " sample gap for testing is characterised by a clear set of electrodes with ideally one or two graphene encapsulated cells bridging the interdigitated electrodes in one location. The presence of any stray graphene bridging the "gap" would quickly discount a potential location. Checking this under FESEM imaging allows us to be absolutely sure that the sample is good for testing to a much higher degree of accuracy than that obtain while attempting to do the same task with a light microscope. Single graphene sheets cannot be seen under a light microscope soa sample selected using a light microscope will typically have to be examined under FESEM after the extensive electrical testing is complete in order ascertain if the data collected was either due to an encapsulated cell sample or a stray graphene sheet bridging the electrode "gap". However, the clear downside of this FESEM exposure

method is that the reduction and examination using the electron beam, combined with exposure to the vacuum in the FESEM will kill the yeast cells on the chip. Therefore, while we have reduced graphene, with do not have a living cell in close proximity to it. This problem is remedied by exposing the cell chip after FESEM to a solution of yeast cells of the stock concentration. Figure 22 above shows the final schematic of the cell-on-cell construct. The goal of this method then is to use the graphene encapsulated dead cell as a method bringing a living cell in contact with a small graphene bridge. Figure 23 below demonstrates the complete cell incubation system. In the background we see the fluidic cell. The pump system draws liquid out of the cell and pumps it around and through a loop submerged in a water bath. The fluid is then reheated and pumped back into the fluid cell which it maintains at 30°C, a temperature conducive to cell growth.
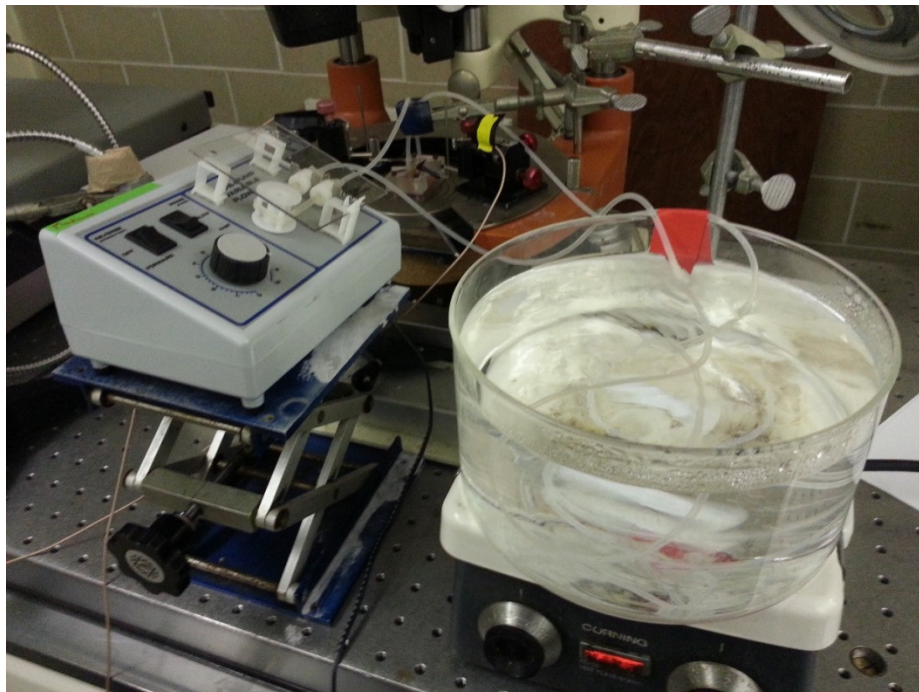

Figure 23: Fluidic cell incubation system.

6.0 Chapter 6- Au-GO-Cell hybrid as a Support for Material Synthesis

The development of new devices at the micro and nano scale require new ideologies and methods with which to attack the problem compared to the top-down approach used in large size scale manufacturing. Making use of all the tools available is of paramount concern to effective research. It is for these reasons that micro-organisms such as viruses, bacteria and the yeast SaC. are of interest. These micro-organisms represent "already manufactured" nano- to micro- templates for the generation of nanodevices.[63] The primary issues with the utilization of micro-organisms in devices are two fold, firstly the formation of a nanostructure on the surface of the cell must not destroy the biological integrity of the organism, and secondly, as we have seen, active integration of the biological response of the micro-organism with the electrical transport in the rest of the device must be attained. However if the micro-organism can be utilized as merely a scaffold, then the Au-GO-Cell Hybrid entity that Kempaiah et al. and we have demonstrated provides an interesting scale on which to construct typical graphene substrate constructs.[55]

As mentioned previously, the dielectric nature of the cell wall of a cell prevents it from being an adequate substrate for electrochemical synthesis in and of itself. However, by coating the SaC cell in graphene we are able to provide a graphene construct suitable for electrochemical synthesis. Additionally, graphene covered yeast cell provides two major features for synthesis, assuming that the structural integrity of the cell-substrate is not damaged during the preparation or synthesis procedures. Firstly the SaC. Cell wall under the graphene layer provides a soft substrate for material growth, and additionally the cell wall is inherently curved providing the potential for radial growth configurations. Since the thickness of a graphene sheet is on the scale of 1-2nm the long range morphology of the cell surface curvature is not impacted.[29,64]

6.1 Material Synthesis on a Curved Substrate

A micron or nano scaled template can be of significant use when attempting to develop new materials and devices. Our graphene encapsulated yeast cells successfully combine the utility of graphene with the curved topography and mechanical softness of the yeast cell wall.[3] This combination makes for an

interesting and more critically, it makes for a curved surface for nanoscale synthesis. The advantage of such a conformation is as follows in Figure 24. As can be seen the typical planar arrangement of ZnO in Figure 24a, the area of photo reception is directly related to the cross-sectional area of the individual nanorod and their packing density. Assuming that the rods in both configurations are packing as tightly and efficiently as possible, the addition of one rod in Figure 24a will only increase the photo excitation area by the cross sectional area of one rod. Comparitively, in Figure 24b and c, when the angle of a successive nanorods is changed from $\theta= 0$, light can interact with both the cross-sectional area as well as the curved area of the rods. Therefore the efficiency of the device rapidly increases with each added rod compared to the planar configuration. As shown numerically in Figure 24c, radial arrangements of zinc nanorod with average widths of 200nm and lengths of 500nm (an under estimate of the eventual material synthesized) at angles of 10° to 45° are adding 200-400% of the contribution that a rod parallel to the original would be able to in a planar system.
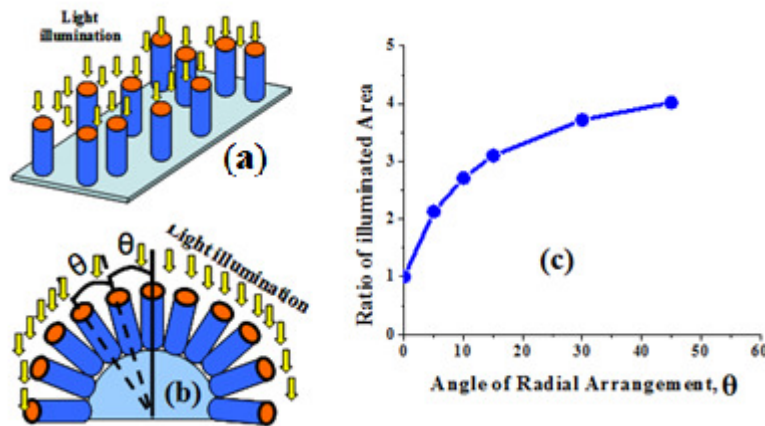

Figure 24: Radial Growth Mechanics a) "Photon capture" area typical of a planar configuration b) "Photon Capture" area of a radial rod configuration c) numerical analysis of the increase in area of the addition[3]
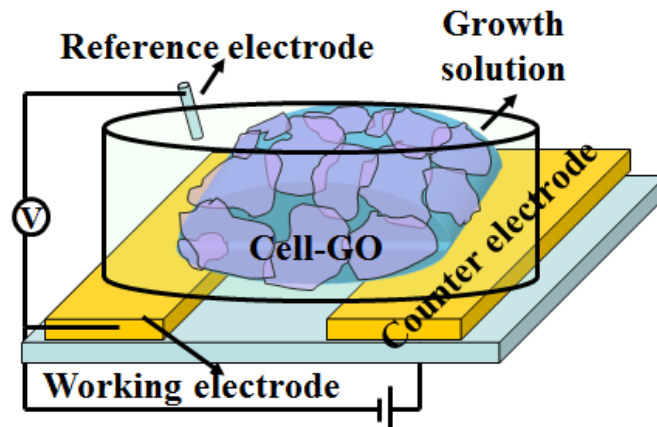
Figure 25: Electrochemical synthesis schematic

6.2 Electrochemical ZnO growth on Graphene

6.2.1 Zinc Oxide growth

Synthesis begins with the Graphene encapsulated Yeast Cells deposited between the inter-digitated electrode array on the previously mentioned gold–array chips. Care is taken to locate specific gaps which express a minimum amount of stray graphene, and distinctly zero graphene bridges that could provide alternative conducting pathways. The gap chosen should also one or a few (depending on the experiment detail) Au-GO-Cell hybrids with a high level of coverage. The selection of gaps, particularly due to the requirement of confirming the appropriate level of graphene coverage necessitated the utilization of a scanning electron microscope (FESEM) as previously used with other projects. As before this simultaneously results in the death of the yeast cells (if not confirmed before) and the reduction of the graphene sheets, improving the conductivity for the electrochemical synthesis.

Once an appropriate chip was selected, the ZnO synthesis method detailed in methods and materials was used to generate the ZnO nano rods on the sample A schematic of the setup in question is provided in Figure 26 as well as the overall proposed process.[3]
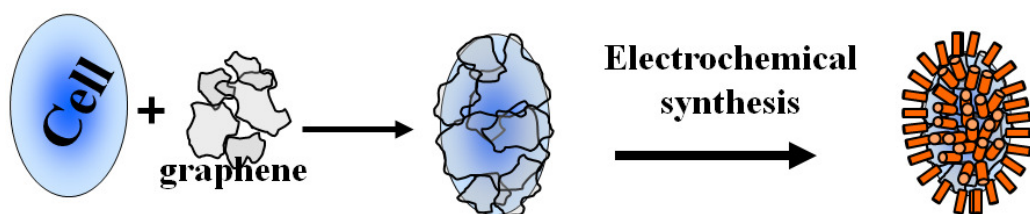
6.2.2 Electrochemical Synthesis- Results

6.2.2.1 Effect of the electrochemical synthesis process on deposited graphene.

To isolate the response of a ZnO Graphene-Cell construct an understanding of secondary effects of the synthesis process must first be attained. An experiment was run where dielectrophoresis was used on a standard gold chip to deposit unreduced graphene oxide sheets in-between the interdigitated electrodes on a gold array chip. Experimentally the set-up look similar to the design of the 3 electrode setup used for ZnO synthesis, minus the reference electrode that is unnecessary in the setup. A cleaned gold array chip, piranha'd and silanized, was viewed under optical microscope to confirm cleanliness. Then a clean gap was selected, and the chip was placed in the microfluidic housing. The fluidic housing would then be filled with 0.9ml of Millipore[TM] water and 0.1ml of 1:40 diluted 2% GO synthesized using our modified hummer's method. An AC voltage of 200mV and 5MOhms is applied across the gap in question for a duration from 10mins to 1hour depending on the amount of Graphene oxide that was wished to be deposited. Figure 27 shows an example of the level of deposition presented by a long exposure time. The sample in question shows significant deposition and multiple stacked layers of graphene on the sample.
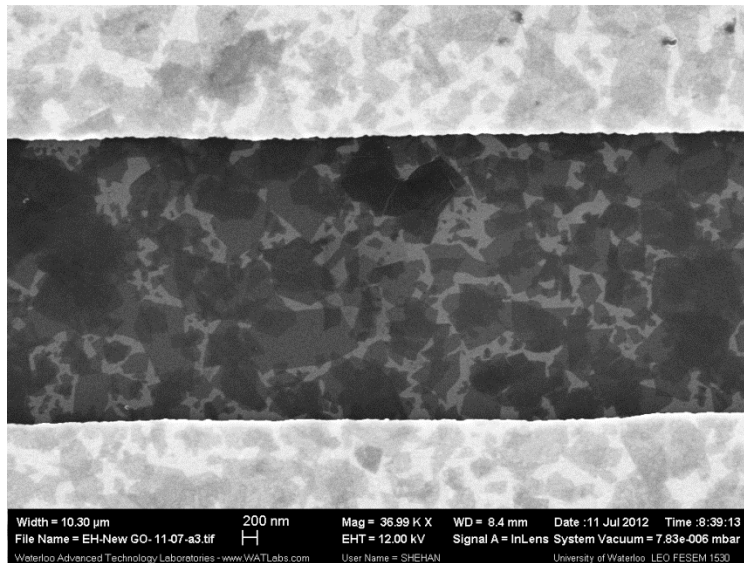
Figure 27: Resulting deposition across an array gap after DEP of graphene oxide

Figure 28 shows ZnO nano rod growth on plain graphene sheets deposited similarly to those seen in Figure 27. A critical characteristic to observe is that ZnO growth in between the electrode digits is constrained only to the locations exhibiting graphene deposition that is connected to the working electrode of the system.[3] Unconnected sheets or graphene sheets connected only to the counter electrode by comparison do not show any growth at all which would support the conclusion that the ZnO growth is due to the electrochemical process used.[3] The rods grown in the image and a hexagonal largest cross section of 150-250nm and the conformation is consistent with growth along the (001) crystallographic surface.[3] This sample was tested for its conductivity and photo electric properties as seen in Figure 31.
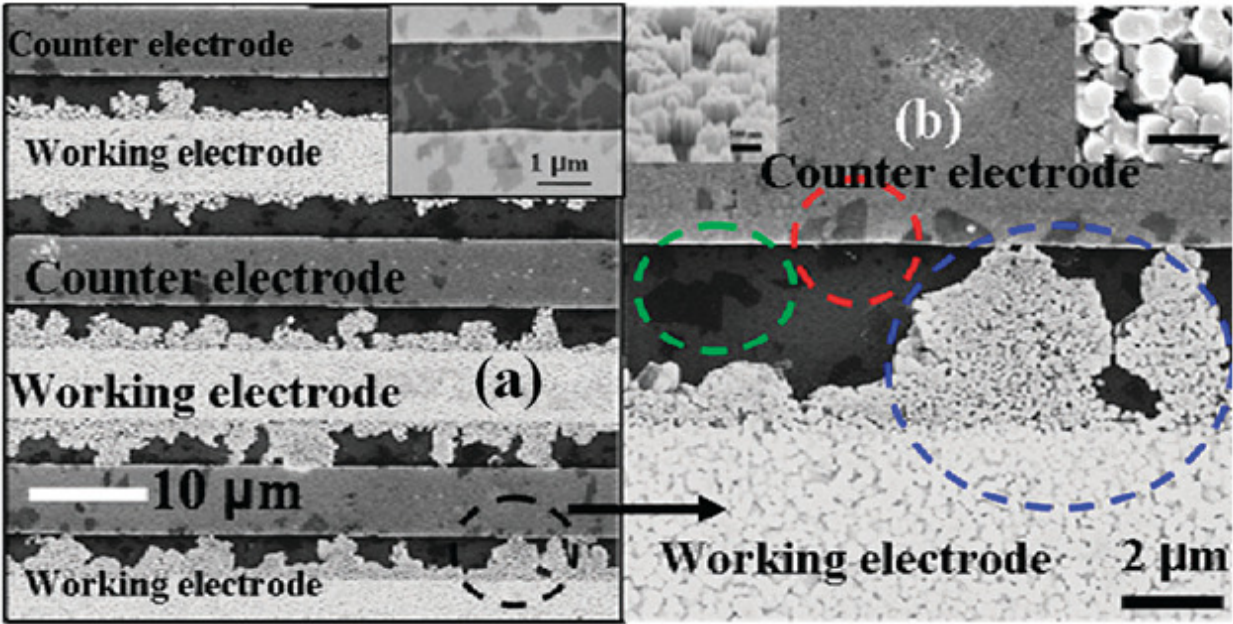
39

6.2.2.2 Electrochemically grown ZnO-GO-SaC. Cell Hybrid constructs.

Electrochemical synthesis was used to grow ZnO on the graphene covered cells. The encapsulating graphene acted as an electrical conductor allowing the induced potential to cover the surface of the otherwise non-conducting cell wall. Figure 29 depicts the ZnO growth seen after synthesis. As seen in the previous graphene oxide sample, the ZnO rods also appear to grow preferentially along the (001) crystallographic plane and express themselves as hexagonal-rods.[3] Figure 29 also shows that, as with the previous san-cells control sample, ZnO only grows on the cells which are connected to the working electrode, supporting the electrochemical synthesis hypothesis that the surface potential of the GO-Cell constructs is critical to the synthesis procedure. Figure 30 below demonstrates a 45° viewing angel FESEM image of the nano-bio-organic hybrid. The grown rods are approximately 1um in length and range from 200nm to 400nm in width.
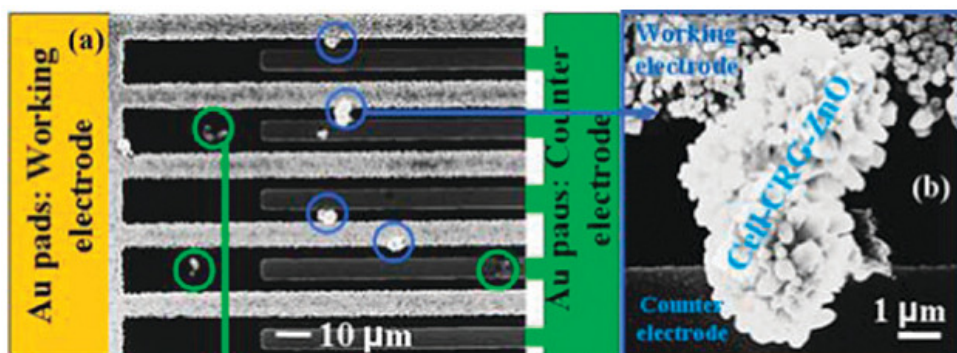
Figure 29:a)Electrochemical ZnO growth on encapsulated Yeast Cells, as before ZnO growth is limited ot those areas in contact with the working electrode b) higher magnification image shows the radial growth direction of the ZnO rods on The encapsulated cell.[3]
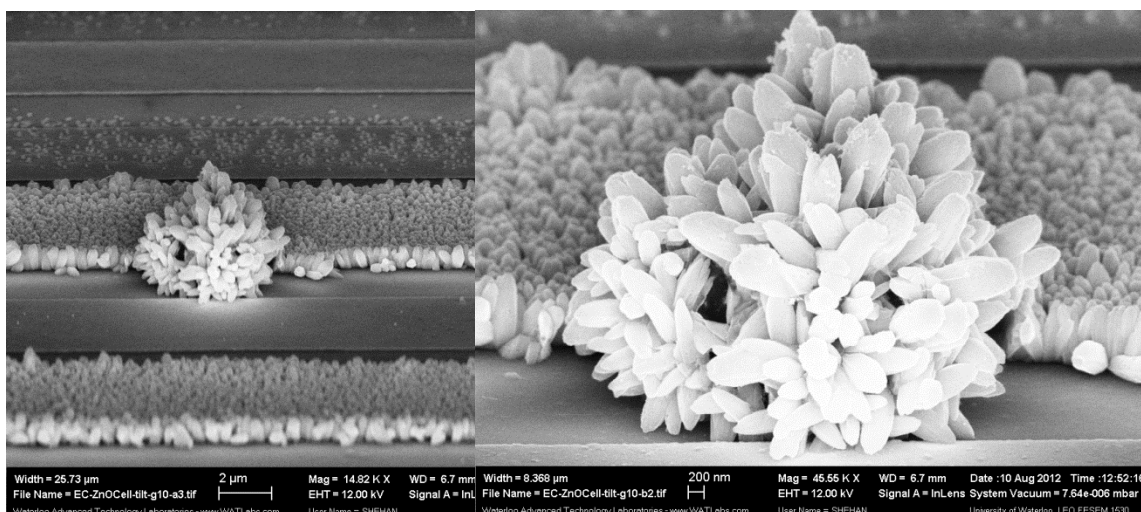
Figure 30: High magnification image of the ERGO-Cell-ZnO construct at a 45° angle. The Radial growth of the ZnO is more clearly seen

Comparing the size of the rods on the graphene-cell to those grown on the working electrode in the background of Figure 30, we can see significant size and morphology differences. The background ZnO rods on the gold working electrode remain more constrained in size since the growth is primarily perpendicular to the gold surface and the width of each rod is then limited by its proximity to its neighbors. Comparatively, the radial growth direction of the ZnO rods on the cell allows for larger rod widths and more varied lengths since as the rods grow outwards the size constraints due to proximal neighbors decrease. Cells appear to remain structurally intact throughout the synthesis process, though it is assumed that they die in the synthesis process. The differences between the morphology of the ZnO in

41

these two cases (on plain graphene oxide sheets versus on the graphene encapsulated cells) can be attributed to the 3D, curved substrate that the cell provides. This same curved morphology also contributes to the differing photo-electric characteristics of the two samples.
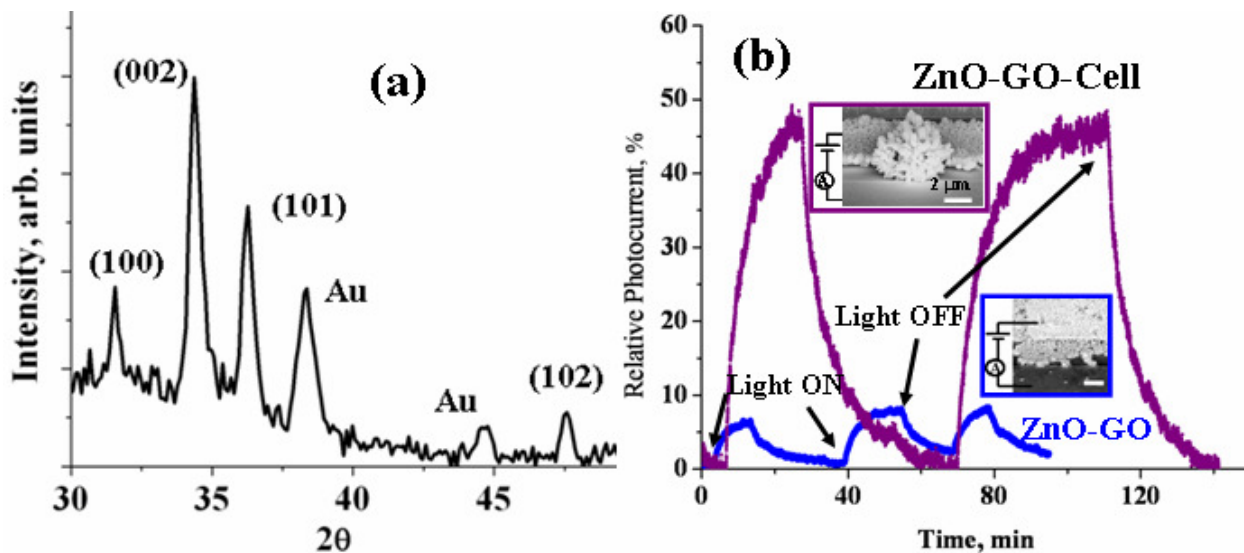
Figure 31: Electrochemically grown ZnO characterization and photoelectric properties a)XRD analysis of the grown material confirms the composition to be that of ZnO. b) Photocurrent characteristics of the ZnO samples indicate an area normalized increase in the photocurrent generated by an encapsulated cell sample above that of a planar sample[3]

Figure 31 shows the comparative photocurrent and XRD data for the two samples. The X-ray diffraction pattern for the synthesized ZnO in Figure 31a confirms the material as ZnO nanorods with primary growth along the (001) crystallographic direction.[3] Regard the electronic testing data in Figure 31b, critically, the curve substrate, that is the electrochemically reduced graphene and cell substrate, exhibits significantly improved performance over its planar compatriot.[3] ZnO is a photosensitive wide band gap semiconductor (~3.2eV) often used.[3] As can be seen in Figure 28 and Figure 29 in certain locations of the gap being tested the only bridges between the two electrodes are due to the deposition of graphene oxide (subsequently converted into electrochemically reduced graphene oxide, henceforth ERGO).[3] In these locations conductance across these bridges is impeded by the number of charge carriers that can be generated by the sample.[3] Comparatively the metal electrodes have an abundance of charge carriers, being conductors. When subjected to illumination with light generated by Newport Arc Lamp Solar Simulator (1.5 solar mass spectrum) electron hole pairs are generated in ZnO.[3,37,47,65] These electrons are injected into the conducting ERGO sheets, while the generated holes become trapped in surface defect states.[3,47,65]

42

This process is what causes the increase in current seen when the samples are exposed to a light source.[3,65] It is assumed that the same process occurring on the ZnO grown on the working electrodes has no current effect, since the metal electrodes are not limited in the charge carriers that can be generated. The graphene sheets are the "bottle neck" to the conductive circuit. As expected, the curved morphology cell-ERGO-ZnO constructs show a much larger ~50% increase in the current compared to the ~8-10% we saw in the planar configuration, a typical value for that flat conformation.[3,65] This compared to a base current of 70-80nA seen for both samples with no light source.[3] It is proposed that this is due to the radial arrangement of the ZnO on the cell samples since this is the most significant difference between the two samples. The relaxation of both the samples is faster than the excitation and on both samples fits a double exponential decay.[3] The time constants for the two samples are correspondingly 6.3 minutes for ERGO-ZnO and 7.8 minutes for the Cell-ERGO-ZnO.[3] The reason for this relaxation time is that the recombination of the holes and electrons trapped in surface oxygen molecules on the ZnO.[3,47,65] When the UV light incident on ZnO is turned off, adsorbed oxygen molecules on the surface of the nanorod capture electrons and convert to O_2^-.[47] When the illumination is then turned back on, photoexcited holes are trapped by the adsorbed O_2^- through surface electron-hole recombination.[47] Subsequent repetition of the same experiment with a long-pass 400nm filter obscuring the illumination gave no photo response, further confirming the observed photo-electric effect.[3]

7.0 Chapter 7- Future work-

7.1 Future work- Cell Sensor

Now that the synthesis method for yeast encapsulation is robust and maximizes graphene coverage while minimizing the amount of stray graphene and stray gold nanoparticles, the next step is to isolate the signal from the noise in the sample. To this end the cell-on-cell device structure has been proposed in combination with the use of a lock in amplifier. The cell-on-cell device structure ensures that a cell comes into contact with a reduced sheet of graphene and also ensures that a gap being tested can be examined under FESEM prior to testing to be sure that any single graphene sheets are not bridging the gap and giving erroneous signals. Prior to this design change there was no way to be sure a cell sample being tested was infact the only sample being tested across a gap. A lock in amplifier will also allow a much more precise reading of the signal from the sample.

7.2 Future work- Graphene encapsulated cells as a substrate for material synthesis

It was clearly shown that a graphene encapsulated cell is a robust substrate for material synthesis. Not only does the underlying cell provide a unique morphology, but the size of the yeast cell could allow for nanoscale structures on a cell to be easily introduced and recovered from various environments. ZnO is naturally anti-bacterial and could have some utility in the photo-degradation of organic molecules. By attaching the ZnO nanorods to a larger cell, potentially a robust, easily filterable cleaning agent has been formed that would be worth investigating. The next step in this idea would be to investigate solution phase ZnO growth mechanisms on encapsulated SaC cells. A potential method for this synthesis would be hydrothermal growth. This low temperature liquid phase methods for the generation of ZnO is simple and high yield and shows no requirement for metal catalysts or templates for growth.[36–38] These methods revolved around seeding growth locations on a substrate and then using hexamethylenetetramine (HTMA) to control growth in a heated zinc nitrate solution.

Another potential avenue for future work could involve expanding the electrochemically synthesized ZnO method to work on not just one cell, but within a cell film. Increasing from one single curved ZnO

substrate to a film of curved substrates could allow for the generation of ZnO solar cells with increased efficacy.

8.0 Chapter 8- Conclusions

Graphene oxide encapsulation provides a base for the development of both cellular sensing and material synthesis methods. In order to refine the encapsulation of the SaC. cells, the previously established encapsulation method of Kempaiah et al. was adjusted to eradicate excess gold on the yeast cells and also to minimize the amount of stray, unattached graphene floating free in the samples. The survivability of cell in the new encapsulation process was confirmed. However, this change to the method requires that cells are encapsulated in graphene oxide which needs to subsequently be reduced to graphene. Un-aided UV reduction was explored but ultimately it proved too inefficient a method for reduction, eventually FESEM exposure was settled on as a fast method to reduce the graphene while also allowing the examinations of testing samples for their suitability before they are tested.

DC testing of the cell samples was examined but ultimately discounted for failing to eliminate sources of noise in the signal; future testing will examine the use of a lock-in amplifier to isolate the cell signal. Modifications to the fluid circulation apparatus were made in attempts to magnify the relevant electrical signal, the flow speed was made more regular to minimize pressure waves pushing through the tubing.

Graphene oxide encapsulated yeast cells were examined for their relevancy as a curved substrate for material synthesis, specifically an electrochemical method for ZnO nanorod growth. The curved substrate that a yeast cell represents helped generate a significantly more effective photocurrent device as the effective surface area than a curved conformation is able to harness is larger. Electrochemical growth resulted in larger nanorods, 200nm to 400nm in width and 1μm in length. Nanorod morphology and XRD analysis confirmed that the material synthesizes was in fact ZnO. Electrochemical growth was confirmed to be dependent on the presence of graphene for success. Explorations into electrochemical growth on a graphene cell film would be a good next avenue to pursue.

References

1.   Smith AM, Ammar R, Nislow C, Giaever G. A survey of yeast genomic assays for drug and target discovery. *Pharmacol Ther*. 2010;127(2):156–64. doi:10.1016/j.pharmthera.2010.04.012.

2.   Hoon S, St Onge RP, Giaever G, Nislow C. Yeast chemical genomics and drug discovery: an update. *Trends Pharmacol Sci*. 2008;29(10):499–504. doi:10.1016/j.tips.2008.07.006.

3.   Tam J, Salgado S, Miltenburg M, Maheshwari V. Electrochemical synthesis on single cells as templates. *Chem Commun (Camb)*. 2013;49(77):8641–3. doi:10.1039/c3cc44308f.

4.   Broach JR, Jones EW, Pringle JR. *The Molecular and Cellular Biology of the Yeast Saccharomyces, Vol. 1. Genome Dynamics, Protein Synthesis, and Energetics*. Cold Spring Harbor, NY: Cold Spring Harbor Laboratory Press; 1991.

5.   Pringle JR, Broach JR, Jones EW. *The Molecular and Cellular Biology of the Yeast Saccharomyces, Vol. 3. Cell cycle and Cell Biology.* Cold Spring Harbor, NY: Cold Spring Harbor Laboratory Press; 1997.

6.   Daum G, Lees ND, Bard M, Dickson R. Biochemistry, cell biology and molecular biology of lipids of Saccharomyces cerevisiae. *Yeast*. 1998;14(16):1471–510. doi:10.1002/(SICI)1097-0061(199812)14:16<1471::AID-YEA353>3.0.CO;2-Y.

7.   Hermann GJ, Shaw JM. Mitochondrial Dynamics. *Annu Rev Cell Dev Biol*. 1998;(14):265–303.

8.   Schneiter R. Genetics, Molecular and Cell Biology of Yeast. 2004;(January). Available at: http://www.unifr.ch/biochem/assets/files/schneiter/cours/Yeast/YeastGenetics.pdf. Accessed December 28, 2014.

9.   Zhang X, Zhang X, He W, et al. High-performance mesoporous $LiFePO_4$ from Baker's yeast. *Colloids Surf B Biointerfaces*. 2013;103:114–20. doi:10.1016/j.colsurfb.2012.10.002.

10.   Wang B, Liu P, Jiang W, Pan H, Xu X, Tang R. Yeast cells with an artificial mineral shell: protection and modification of living cells by biomimetic mineralization. *Angew Chem Int Ed Engl*. 2008;47(19):3560–4. doi:10.1002/anie.200704718.

11.   Lesage G, Bussey H. Cell wall assembly in Saccharomyces cerevisiae. *Microbiol Mol Biol Rev*. 2006;70(2):317–43. doi:10.1128/MMBR.00038-05.

12.   Kempaiah R, Salgado S, Chung WL, Maheshwari V. Graphene as membrane for encapsulation of yeast cells: protective and electrically conducting. *Chem Commun (Camb)*. 2011;47(41):11480–2. doi:10.1039/c1cc15096k.

13.   Functional Technologies Corp. - About Yeast. Available at: http://www.functionaltechcorp.com/s/Yeast.asp. Accessed January 30, 2014.

14.   Carter JL. Band Structure of Graphite. *J Chem Phys*. 1953;21(12):492. doi:10.1063/1.1698840.

15.   Geim a K, Novoselov KS. The rise of graphene. *Nat Mater*. 2007;6(3):183–91. doi:10.1038/nmat1849.

16.   Singh V, Joung D, Zhai L, Das S, Khondaker SI, Seal S. Graphene based materials: Past, present and future. *Prog Mater Sci*. 2011;56(8):1178–1271. doi:10.1016/j.pmatsci.2011.03.003.

17.   Gan T, Hu S. Electrochemical sensors based on graphene materials. *Microchim Acta*. 2011;175(1-2):1–19. doi:10.1007/s00604-011-0639-7.

18.   Sahoo S. Quantum Hall effect in graphene : Status and prospects. *Indian J Pure Appl Phys*. 2011;49(June):367–371.

19.   Park KS. Topological effects, index theorem and supersymmetry in graphene. *Quantum*. 2010:1–26.

20.   Ghosh S, Bao W, Nika DL, et al. Dimensional crossover of thermal transport in few-layer graphene. *Nat Mater*. 2010;9(7):555–558. doi:10.1038/nmat2753.

21.   Huang M, Pascal T a, Kim H, Goddard W a, Greer JR. Electronic--mechanical coupling in graphene from in situ nanoindentation experiments and multiscale atomistic simulations. *Nano Lett*. 2011;11(3):1241–6. doi:10.1021/nl104227t.

22.   Castro Neto a., Guinea F, Peres N, Novoselov K, Geim a. The electronic properties of graphene. *Rev Mod Phys*. 2009;81(1):109–162. doi:10.1103/RevModPhys.81.109.

23.   Sahoo S. Quantum Hall effect in graphene : Status and prospects. *Indian J Pure Appl Phys*. 2011;49(June):367–371.

24.   Zhu Y, Murali S, Cai W, et al. Graphene and graphene oxide: synthesis, properties, and applications. *Adv Mater*. 2010;22(35):3906–24. doi:10.1002/adma.201001068.

25.   Schedin F, Geim a K, Morozov S V, et al. Detection of individual gas molecules adsorbed on graphene. *Nat Mater*. 2007;6(9):652–5. doi:10.1038/nmat1967.

26.   Kim K, Choi J-Y, Kim T, Cho S-H, Chung H-J. A role for graphene in silicon-based semiconductor devices. *Nature*. 2011;479(7373):338–44. doi:10.1038/nature10680.

27.   Bolotin K, Sikes K, Hone J, Stormer H, Kim P. Temperature-Dependent Transport in Suspended Graphene. *Phys Rev Lett*. 2008;101(9):1–4. doi:10.1103/PhysRevLett.101.096802.

28.   Chen F, Qing Q, Xia J, Tao N. Graphene field-effect transistors: electrochemical gating, interfacial capacitance, and biosensing applications. *Chem Asian J*. 2010;5(10):2144–53. doi:10.1002/asia.201000252.

29.   Ma H, Wu D, Cui Z, et al. Graphene-Based Optical and Electrochemical Biosensors: A Review. *Anal Lett*. 2013;46(1):1–17. doi:10.1080/00032719.2012.706850.

30.   Alwarappan S, Liu C, Kumar A, Li C-Z. Enzyme-Doped Graphene Nanosheets for Enhanced Glucose Biosensing. *J Phys Chem C*. 2010;114(30):12920–12924. doi:10.1021/jp103273z.

31.   Artiles MS, Rout CS, Fisher TS. Graphene-based hybrid materials and devices for biosensing. *Adv Drug Deliv Rev*. 2011;63(14-15):1352–60. doi:10.1016/j.addr.2011.07.005.

32.   Huang Y, Chen P. Nanoelectronic biosensing of dynamic cellular activities based on nanostructured materials. *Adv Mater*. 2010;22(25):2818–23. doi:10.1002/adma.200904235.

33.   Dong X, Shi Y, Huang W, Chen P, Li L-J. Electrical detection of DNA hybridization with single-base specificity using transistors based on CVD-grown graphene sheets. *Adv Mater*. 2010;22(14):1649–53. doi:10.1002/adma.200903645.

34.   Yang W, Ratinac KR, Ringer SP, Thordarson P, Gooding JJ, Braet F. Carbon nanomaterials in biosensors: should you use nanotubes or graphene? *Angew Chem Int Ed Engl*. 2010;49(12):2114–38. doi:10.1002/anie.200903463.

35.   He Q, Sudibya HG, Yin Z, et al. Micropatterns of Reduced Graphene Oxide Films : Fabrication and Sensing Applications. 2010;4(6):3201–3208.

36.   Baruah S, Dutta J. Hydrothermal growth of ZnO nanostructures. *Sci Technol Adv Mater*. 2009;10(1):013001. doi:10.1088/1468-6996/10/1/013001.

37.   Cheng B, Samulski ET. Hydrothermal synthesis of one-dimensional ZnO nanostructures with different aspect ratios. *Chem Commun (Camb)*. 2004;(8):986–7. doi:10.1039/b316435g.

38.   Jung HJ, Lee S, Yu Y, Hong SM, Choi HC, Choi MY. Low-temperature hydrothermal growth of ZnO nanorods on sol–gel prepared ZnO seed layers: Optimal growth conditions. *Thin Solid Films*. 2012;524:144–150. doi:10.1016/j.tsf.2012.10.007.

39.   Wang ZL. Zinc oxide nanostructures: growth, properties and applications. *J Phys Condens Matter*. 2004;16(25):R829–R858. doi:10.1088/0953-8984/16/25/R01.

40.   Janotti A, Van de Walle CG. Fundamentals of zinc oxide as a semiconductor. *Reports Prog Phys*. 2009;72(12):126501. doi:10.1088/0034-4885/72/12/126501.

41.   Zhou W, Zhang X, Zhao D, Gao M, Xie S. ZnO nanorods: morphology control, optical properties, and nanodevice applications. *Sci China Physics, Mech Astron*. 2013;56(12):2243–2265. doi:10.1007/s11433-013-5350-8.

42.   Klingshirn C. ZnO: From basics towards applications. *Phys Status Solidi*. 2007;244(9):3027–3073. doi:10.1002/pssb.200743072.

43.   Das S, Ghosh S. Fabrication of different morphologies of ZnO superstructures in presence of synthesized ethylammonium nitrate (EAN) ionic liquid: synthesis, characterization and analysis. *Dalton Trans*. 2013;42(5):1645–56. doi:10.1039/c2dt31920a.

44.   Panda D, Tseng T-Y. One-dimensional ZnO nanostructures: fabrication, optoelectronic properties, and device applications. *J Mater Sci*. 2013;48(20):6849–6877. doi:10.1007/s10853-013-7541-0.

45.   Djurisić AB, Leung YH. Optical properties of ZnO nanostructures. *Small*. 2006;2(8-9):944–61. doi:10.1002/smll.200600134.

46.   Heo YW, Norton DP, Tien LC, et al. ZnO nanowire growth and devices. *Mater Sci Eng R Reports*. 2004;47(1-2):1–47. doi:10.1016/j.mser.2004.09.001.

47.   Bera a., Basak D. Role of defects in the anomalous photoconductivity in ZnO nanowires. *Appl Phys Lett*. 2009;94(16):163119. doi:10.1063/1.3123167.

48.   Xia Y, Yang P, Sun Y, et al. One-Dimensional Nanostructures: Synthesis, Characterization, and Applications. *Adv Mater*. 2003;15(5):353–389. doi:10.1002/adma.200390087.

49. Greene LE, Law M, Tan DH, et al. General route to vertical ZnO nanowire arrays using textured ZnO seeds. *Nano Lett*. 2005;5(7):1231–6. Available at: http://www.ncbi.nlm.nih.gov/pubmed/16178216.

50. Kovtyukhova NI, Ollivier PJ, Martin BR, et al. Layer-by-Layer Assembly of Ultrathin Composite Films from Micron-Sized Graphite Oxide Sheets and Polycations. *Chem Mater*. 1999;11(3):771–778. doi:10.1021/cm981085u.

51. Pohl HA. *Dielectrophoresis: The behaviour of neutral matter in non-uniform electric fields*. Cambridge: Cambridge University Press; 1978.

52. Díaz R, Payen S. Biological cell separation using dielectrophoresis in a microfluidic device. :1–4. Available at: http://robotics.eecs.berkeley.edu/~pister/245/project/DiazPayen.pdf. Accessed January 6, 2014.

53. Jones TB. Basic Theory of Dielectrophoresis and Electrorotation. *IEEE Eng Med Biol*. 2003;(December):33–42.

54. Dimaki M, Bøggild P. Dielectrophoresis of carbon nanotubes using microelectrodes: a numerical study. *Nanotechnology*. 2004;15(8):1095–1102. doi:10.1088/0957-4484/15/8/039.

55. Kempaiah R, Maheshwari V. Graphene as Cellular Interface : Electromechanical Coupling with cells. *Yeast*. 200. doi:10.1002/anie.200)).

56. Kempaiah R. Electromechanical Coupling of Graphene With Cells. 2011.

57. Zhang H, Liu Q, Feng K, Chen B, Tung C, Wu L. Facile Photoreduction of Graphene Oxide by an NAD(P)H Model: Hantzsch 1,4-Dihydropyridine. 2012.

58. Paredes JI, Martı A, Tasco JMD. Graphene Oxide Dispersions in Organic Solvents. *Langmuir*. 2008;(18):10560–10564.

59. Wu T, Liu S, Luo Y, Lu W, Wang L, Sun X. Surface plasmon resonance-induced visible light photocatalytic reduction of graphene oxide: using Ag nanoparticles as a plasmonic photocatalyst. *Nanoscale*. 2011;3(5):2142–4. doi:10.1039/c1nr10128e.

60. Xue Y, Liu Y, Lu F, Qu J, Chen H, Dai L. Functionalization of Graphene Oxide with Polyhedral Oligomeric Silsesquioxane (POSS) for Multifunctional Applications. *J Phys Chem Lett*. 2012;3(12):1607–1612. doi:10.1021/jz3005877.

61. Wang X, Li X, Zhang L, et al. N-doping of graphene through electrothermal reactions with ammonia. *Science*. 2009;324(5928):768–71. doi:10.1126/science.1170335.

62. Jahanshahi M, Rashidi AM, Ghoreyshi AA. Synthesis and Characterization of Thermally-Reduced Graphene 1. 2013;4(1):53–59. doi:10.5829/idosi.ijee.2013.04.01.09.

63. Berry V, Saraf RF. Self-assembly of nanoparticles on live bacterium: an avenue to fabricate electronic devices. *Angew Chem Int Ed Engl*. 2005;44(41):6668–73. doi:10.1002/anie.200501711.

64. Pumera M, Ambrosi A, Bonanni A, Chng ELK, Poh HL. Graphene for electrochemical sensing and biosensing. *TrAC Trends Anal Chem*. 2010;29(9):954–965. doi:10.1016/j.trac.2010.05.011.

65. Chang H, Sun Z, Ho KY-F, et al. A highly sensitive ultraviolet sensor based on a facile in situ solution-grown ZnO nanorod/graphene heterostructure. *Nanoscale*. 2011;3(1):258–64. doi:10.1039/c0nr00588f.

Appendix A

Gold Patterned SiO₂ Chip
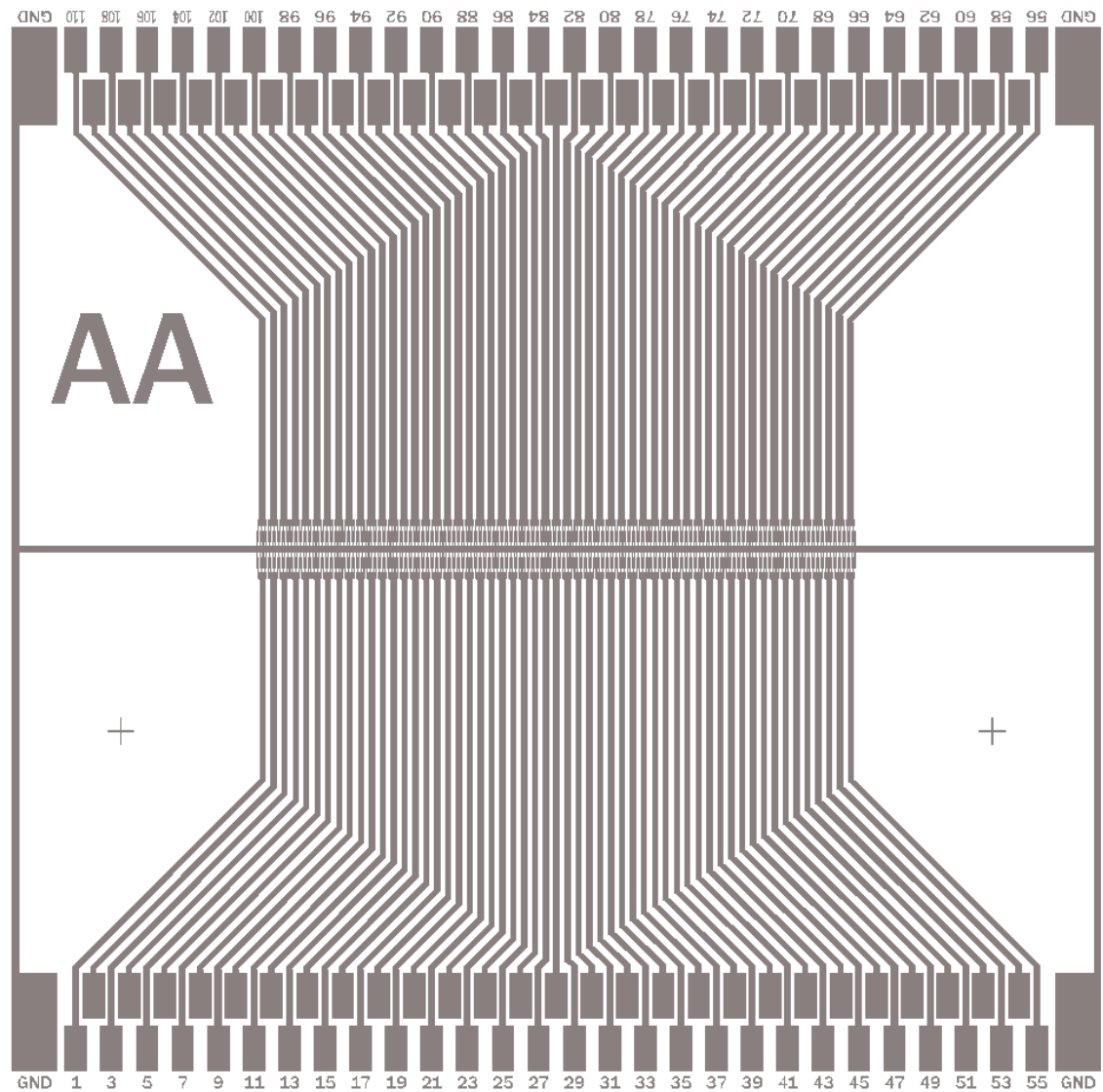
The mask shows the areas of the chip where the gold layer will be deposited. The chip is composed of 110 "gaps" each with 6 interdigitated electrodes connected to a "pad" on the outer edge of the chip. The centre ground connects to "pads" in all 4 corners.

Glossary

APTES- (3-Aminopropyl)triethoxysilane

Au-Go-Cell- Graphene Oxide encapsulated cell

ERGO- electrochemically reduced graphene

FESEM- Field Emission Scanning Electron Microscope

FET- field effect transistor

GO- Graphene Oxide

Gold Chip- Gold electrode chip on a Silicon dioxide base

NP- nanoparticles

SaC.- Saccharomyces cerevisiae

XRD- X-Ray Diffraction

ZnO- Zinc oxide